(p)ppGpp and moonlighting RNases influence the first step of lipopolysaccharide biosynthesis in *Escherichia coli*

Simon Brückner [1], Fabian Müller[1], Laura Schadowski[1], Tyll Kalle[1], Sophia Weber[1], Emily C. Marino [1], Blanka Kutscher[1], Anna-Maria Möller[1], Sabine Adler[2], Dominik Begerow[2,3], Wieland Steinchen[4], Gert Bange [4], Franz Narberhaus [1,*]

[1]Microbial Biology, Faculty of Biology and Biotechnology, Ruhr University Bochum, Universitätsstrasse 150, Bochum, Germany
[2]Evolution of Plants and Fungi, Faculty of Biology and Biotechnology, Ruhr University Bochum, Universitätsstrasse 150, Bochum, Germany
[3]Organismische Botanik und Mykologie, Institut für Planzenwissenschaften und Mikrobiologie, Fachbereich Biologie, Universität Hamburg, Ohnhorststrasse 18, Hamburg, Germany
[4]Center for Synthetic Microbiology (SYNMIKRO) and Department of Chemistry, Philipps-University Marburg, Karl-von-Frisch-Strasse 14, Marburg, Germany
*Corresponding author. Faculty of Biology and Biotechnology**,** Microbial Biology**,** Ruhr University Bochum, Universitätsstrasse 150, NDEF 06/784**,** 44780 Bochum, Germany. Tel: +492343223100; Fax: +492343214620; E-mail: franz.narberhaus@rub.de
Editor: [Anke Becker]

Abstract

The outer membrane (OM) protects Gram-negative bacteria from harsh environmental conditions and provides intrinsic resistance to many antimicrobial compounds. The asymmetric OM is characterized by phospholipids in the inner leaflet and lipopolysaccharides (LPS) in the outer leaflet. Previous reports suggested an involvement of the signaling nucleotide ppGpp in cell envelope homeostasis in *Escherichia coli*. Here, we investigated the effect of ppGpp on OM biosynthesis. We found that ppGpp inhibits the activity of LpxA, the first enzyme of LPS biosynthesis, in a fluorometric *in vitro* assay. Moreover, overproduction of LpxA resulted in elongated cells and shedding of outer membrane vesicles (OMVs) with altered LPS content. These effects were markedly stronger in a ppGpp-deficient background. We further show that RnhB, an RNase H isoenzyme, binds ppGpp, interacts with LpxA, and modulates its activity. Overall, our study uncovered new regulatory players in the early steps of LPS biosynthesis, an essential process with many implications in the physiology and susceptibility to antibiotics of Gram-negative commensals and pathogens.

Keywords: outer membrane, LpxA, outer membrane vesicles, RNase H, RnhB, moonlighting, phospholipid biosynthesis, peptidoglycan biosynthesis, stringent response

Introduction

In *Escherichia coli*, the signaling molecules guanosine tetraphosphate (ppGpp) and guanosine pentaphosphate (pppGpp) collectively referred to as (p)ppGpp, play a fundamental role in metabolic adaptation to nutrient deprivation and environmental stress. Synthesized by RelA and SpoT (Fig. 1A), intracellular ppGpp levels increase to ∼1 mM during the transition to stationary phase, ∼25 times higher than during exponential phase (Varik et al. 2017). In addition to globally altering transcription by interacting with RNA polymerase and DksA, (p)ppGpp can bind to numerous biosynthetic enzymes, in most cases to inhibit them (Kanjee et al. 2012, Zhang et al. 2018, Wang et al. 2019). Metabolic pathways remodeled by (p)ppGpp include but are not limited to nucleotide synthesis, DNA replication, ribosome maturation and function, lipid metabolism, and bacterial pathogenesis (Anderson et al. 2021, Irving et al. 2021). Recently, a sequential shutdown program has been postulated, in which low levels of (p)ppGpp affect nonessential metabolic pathways. Essential pathways such as replication or fatty acid biosynthesis are inhibited only at high (stringent) (p)ppGpp concentrations (Steinchen et al. 2020). Given the high number of cellular (p)ppGpp binders, it has been argued that the (p)ppGpp signaling pathway should be a primary focus of antimicrobial therapy since its inactivation would interfere with many fundamental processes simultaneously (Pulschen et al. 2021).

Most enzymes responsible for the biosynthesis of the inner membrane (IM), the cell wall, and the outer membrane (OM) of *E. coli* are essential because these three layers protect the bacterium from external stress. The Gram-negative OM has an asymmetric structure with phospholipids (PL) in the inner leaflet and lipopolysaccharides (LPS) in the outer leaflet (Silhavy et al. 2010, Lundstedt et al. 2021). This highly effective barrier confers intrinsic antibiotic resistance to many Gram-negative human pathogens. The lipid A portion of LPS anchors it to the membrane, and when released, it acts as a pyrogen in eukaryotic cells, commonly known as endotoxin. It is important to note that excessive levels of LPS can also be harmful to the bacteria themselves because it results in abnormal membrane structures in the periplasm (Ogura et al. 1999). Therefore, balancing the synthesis of PL and LPS is critical to preventing toxicity. Both pathways share the precursor molecule acyl-[acyl carrier protein] (acyl-ACP), which is delivered towards PL or LPS biosynthesis by FabZ or by LpxA/LpxC, respectively (Anderson et al. 1993). At physiological ppGpp concentrations (∼1 mM), FabZ activity is reduced to ∼70% *in vitro* (Stein and Bloch 1976), suggesting that ppGpp acts as an inhibitor of PL biosynthesis. We hypothesized that (p)ppGpp also inhibits LpxA catalyzing the first, but thermodynamically unfavorable, step of LPS biosynthesis. LpxC, the second enzyme in the pathway, has long been the focus of attention because it catalyzes the first committed step. The protease FtsH degrades LpxC
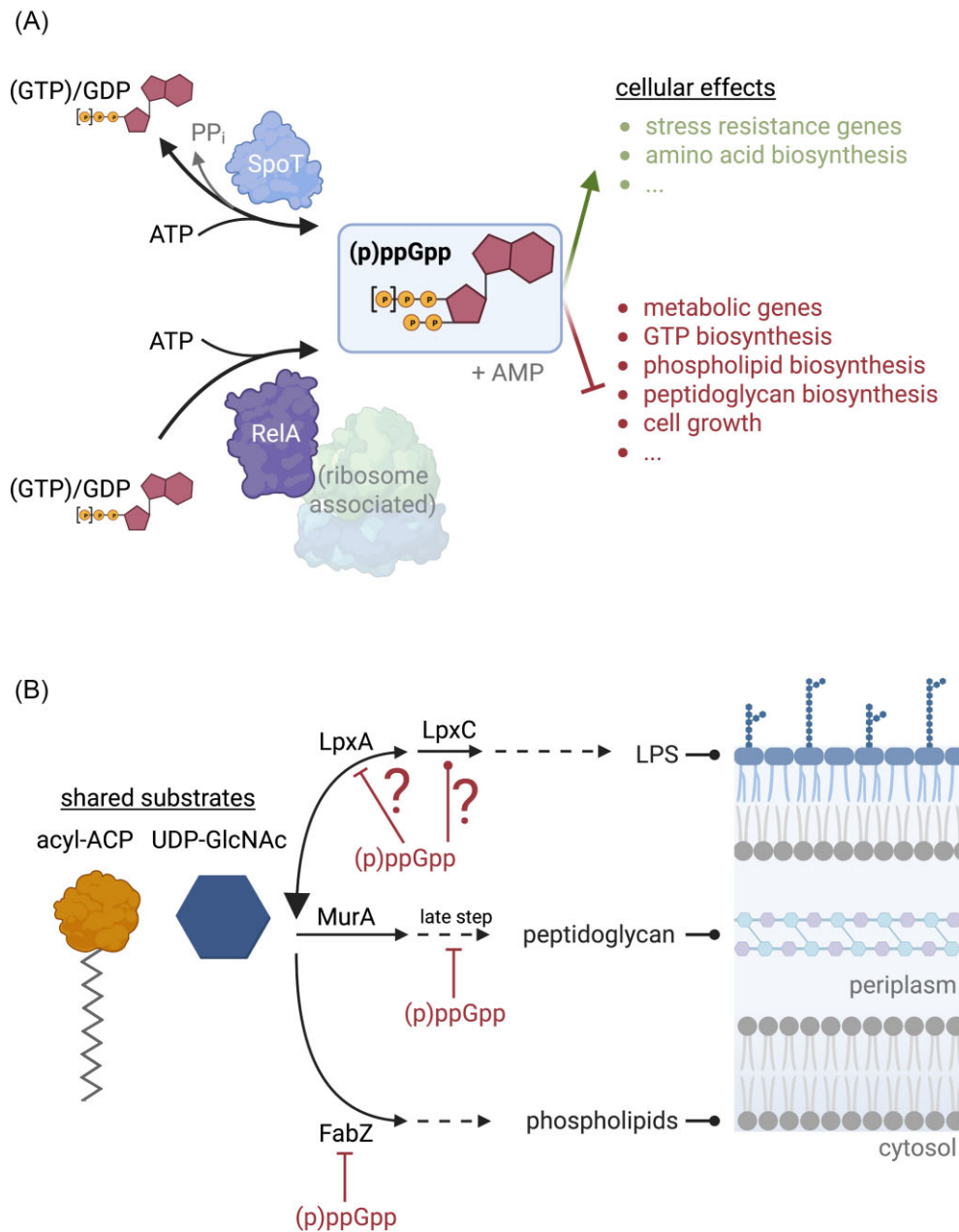
Figure 1. Physiological consequences of the stringent response in *E. coli*. **(A)** The global signaling nucleotides (p)ppGpp are produced in millimolar amounts in response to various environmental stressors and orchestrate metabolic reprogramming of the cell (Irving et al. 2021). **(B)** The biosynthetic pathways of lipopolysaccharides (LPS), peptidoglycan (PGN), and phospholipids (PL) are linked by sharing the same substrates. Acyl-ACP can be consumed by the LPS and PL pathways, while UDP-GlcNAc can be consumed by the LPS and PGN pathways. It is known that the biosynthesis of PGN and PL is inhibited by (p)ppGpp (Stein and Bloch 1976, Ramey and Ishiguro 1978).

at slow growth rates to prevent toxic LPS excess, while LpxC is stable during rapid growth. In a (p)ppGpp[0] mutant, LpxC degradation is reversed, suggesting that (p)ppGpp may directly affect LPS biosynthesis (Schäkermann et al. 2013).

The *rnhB* gene is encoded in the same operon immediately downstream of *lpxD*, *fabZ*, *lpxA*, and *lpxD*, although its gene product has no apparent role in LPS biosynthesis. Apart from the primary RnhA (RNase HI), RnhB (RNase HII) is the second RNase H in *E. coli* (Itaya 1990). RNase H enzymes cleave the RNA strand in DNA:RNA hybrids during replication and excision repair. Interestingly, a proteome-wide pull-down screen revealed an interaction between RnhB and LpxA (Arifuzzaman et al. 2006). In addition, RnhB was recently shown to enhance the enzymatic activity of the

uridine diphosphate (UDP)–glucose dehydrogenase Ugd, which is involved in LPS modification and colanic acid biosynthesis (Rodionova et al. 2020). These interactions suggest "moonlighting" functions of RnhB in LPS biosynthesis.

Abovementioned findings prompted us to examine the interplay between early LPS biosynthesis enzymes, (p)ppGpp and RnhB in *E. coli*. Previous global protein–ligand interaction screens did not report any (p)ppGpp-binding proteins in the LPS pathway (Zhang et al. 2018, Wang et al. 2019). Our study demonstrates that both (p)ppGpp and RNase H enzymes influence the substrate flux into the LPS biosynthesis pathway and provide a new perspective on the regulation of this essential process.

Material and methods

Materials

$^{\gamma P32}$adenosine triphosphate (ATP) was purchased from Hartmann Analytic GmbH. *Vibrio harveyi* ATCC14126 genomic DNA (gDNA) was obtained from the DSMZ-German Collection of Microorganisms and Cell Cultures GmbH. *R*-3-hydroxymyristic acid ((*R*)-3-hydroxytetradecanoic acid) and ThioGlo® 1 (methyl 10-(2,5-dioxo-2,5-dihydro-1H-pyrrol-1-yl)-9-methoxy-3-oxo-3*H*-benzo[*f*]chromene-2-carboxylate) were from abcr. Uridine-diphosphate-*N*-acetylglucosamine (UDP-GlcNAc) and SYPRO™ Orange protein gel stain were purchased from Sigma. All other chemicals were analytical grade.

Bacterial strains and culture conditions

Bacterial strains and plasmids are listed in Table S1 (Supporting Information). A single colony of *E. coli* was used to inoculate 1–5 ml of lysogeny broth (LB, 10 g/l NaCl, 10 g/l bacto-tryptone, and 5 g/l yeast extract) supplemented with appropriate antibiotics (working concentrations were 100 μg/ml ampicillin, 50 μg/ml kanamycin, and 30 μg/ml chloramphenicol). After ∼18 h shaking at 37°C, the culture was used to inoculate fresh medium with the respective antibiotics at an optical density at 600 nm (OD_{600}) of 0.05. TSS solution was used to make the cells chemically competent (Chung et al. 1989).

Construction of expression plasmids

The plasmids and oligonucleotides used in this study are listed in Tables S1 and S2 (Supporting Information), respectively. The amino acid sequences of the fusion proteins that were generated in this study are listed in Table S3 (Supporting Information). PCR products were generated using Phusion High-Fidelity PCR Master Mix with HF Buffer (Thermo Scientific™) according to the manufacturer's instructions. DNA fragments were cloned either by BsaI-mediated restriction of the PCR product and vector and simultaneous ligation at room temperature (RT) overnight or by using the NEBuilder® HiFi DNA Assembly Master Mix (New England Biolabs) according to the manufacturer's instructions using PCR-linearized plasmid. For pBO4885, the PCR products amplified with SB151 and SB152 and pACYCDuet-1 (Novagen) were digested with NcoI and AflII and joined by ligation. The PCR products amplified with SB153 and SB154, and pBO4885 were digested with NdeI and AvrII and ligated to form the coexpression plasmid pBO4886. *Escherichia coli* TOP10 cells were used as the cloning host, and recombinant DNA techniques were performed according to standard protocols (Sambrook and Russell 2001).

All oligonucleotides were purchased from Eurofins. The molecular beacon SB225 was designed according to the previously described beacon 6 (Rizzo et al. 2002).

Growth curve analysis and immunological detection of proteins

Growth curves were recorded using a Tecan Infinite® M Plex microplate reader. Overnight cultures were prepared as described and used to inoculate fresh LB medium (without antibiotics) at an OD_{600} of 0.02. 200 μl were added to each well of a 96-well plate, and the plate was sealed with a Breathe-Easy® breathable sealing membrane (Diversified Biotech). Bacteria were allowed to grow for 105 min at 37°C (shaking), and OD_{600} measurements were taken every 13 min. Anhydrotetracycline (AHT) was added to a final concentration of 50 ng/ml to induce protein overproduction. The plate was resealed with Breathe-Easy®, and bacte-

rial growth was monitored overnight at 37°C. Successful protein production was confirmed by dot-blot analysis. The microplate was centrifuged (10 min, 4000 × *g*, 4°C), the culture supernatant was removed, and the cells were resuspended in 50 μl of lysis buffer A2 (Macherey-Nagel). After 5 min at RT, 3 μl of cell lysate from each well was spotted on a nitrocellulose membrane and allowed to dry. After blocking for 1 h at RT in blocking buffer (3% BSA in tris-buffered saline (TBS) with Tween 20 (TBST), sterile filtered), rabbit antistrep-tag polyclonal antibody (Invitrogen, PA5-114454) was added at 1:4000 and incubated for 1 h at RT. The membrane was rinsed and washed three times for 5 min with TBST, and goat–antirabbit ECL plex IgG-Cy5 (Amersham) was added at 1:4000 in blocking buffer. After 1 h at RT, the membrane was rinsed and washed three times for 5 min in TBST, rinsed with TBS, and imaged using a ChemiDoc™ MP imaging system (Bio-Rad).

Microscopy for determination of cell length

Bacteria were grown as described for growth curve analysis. After 18 h of growth, cells were pelleted (1 min, 11 000 × *g*, RT) and resuspended in a sixth volume of 0.9% NaCl (w/v). 5 μl of this cell suspension was spotted on an agarose patch [1.5% agarose (w/v) in 0.9% NaCl] on a microscope slide, covered with a coverslip, and cells were analyzed in brightfield using an Olympus BX51 fluorescence microscope at 60 × magnification (oil immersion lens). Cell length was quantified using ImageJ.

Determination of OM permeability

The fluorescent probe *N*-phenyl-1-naphthylamine (NPN; Sigma) was used to determine changes in OM permeability in response to protein overproduction. Overnight cultures (with appropriate antibiotics) were used to inoculate the main cultures (20 ml of LB without antibiotics in 100 ml Erlenmeyer flasks) to an OD_{600} of 0.02. Cultures were allowed to grow in a shaking water bath at 37°C for 105 min, and overexpression was induced by addition of 50 ng/ml AHT. Protein was overproduced for 3 h. Cells were harvested and resuspended in 5 mM 4-(2-hydroxyethyl)piperazine-1-ethanesulfonic acid (HEPES) at pH 7 to an OD_{600} of 1. Cells were then subjected to the NPN uptake assay as previously described (Helander and Mattila-Sandholm 2000). 1 mM EDTA was included as a positive control for membrane permeabilization. The NPN uptake factors were determined, and wildtype (WT) cells carrying the EV were normalized to 1.

Determination of cellular steady-state LPS levels

Overnight cultures were used to inoculate 10 ml of LB (without antibiotics) to an OD_{600} of 0.05. Cultures were incubated at 37°C in a shaking water bath. OD_{600} was determined hourly. Samples were collected at specific time points. For exponential cells, an OD_{600} of 0.5 was used; for transition cells, when growth had just ceased exponential growth, and for stationary cells, cells grown overnight were used. In each case, 1 ml of the bacterial culture was collected and centrifuged (1 min, 13 200 rpm, RT). The supernatant was removed, and the cell pellet was stored at −20°C. The cell pellets were resuspended in TE buffer (OD_{600} of 1 = 100 μl). The samples were mixed with SDS sample buffer and boiled (10 min, 95°C). Samples were centrifuged (2 min, 13 200 rpm, RT) and loaded onto a 12% TGX Stain-Free™ gel. Electrophoresis was performed at 200 V until the running front reached approximately three-quarters of the gel. In the ChemiDoc™ MP (Bio-Rad), the gels were UV activated for 45 s using the Stain-Free™ program to visualize total protein. Western transfer (Trans-Blot® Turbo™

with nitrocellulose consumables, Bio-Rad) was followed by a 5-min blocking step in EveryBlot blocking buffer (Bio-Rad). Mouse antilipopolysaccharide core monoclonal antibody mAb WN1 222–5 (Hycult Biotech) was added at a dilution of 1:4000 and incubated for 1 h at RT. After the membrane was rinsed three times with TBST and washed four times for 5 min each in TBST, the secondary antibody StarBright Blue 700 Goat Anti-Mouse IgG (Bio-Rad) at a dilution of 1:2500 in EveryBlot blocking buffer was added to the membrane for 1 h. After repeated washes, the membrane was dried, and the fluorescence signals of total protein (Stain-Free™ channel) and core LPS (StarBright Blue 700 channel) were detected. Using ImageLab software (Bio-Rad), the signal intensities of the core LPS bands were determined and normalized to total protein.

Isolation of outer membrane vesicles

Cells were cultured as described for growth curve analysis, but in 50 ml of LB in a 250 ml Erlenmeyer flask. After 20 h of growth and protein overproduction, cultures were OD_{600} normalized by adding fresh LB. Sodium dodecyl sulfate polyacrylamide gel electrophoresis (SDS-PAGE), Western transfer, and immunological detection of the strep tag verified successful protein overproduction. The ExoBacteria™ outer membrane vesicle (OMV) isolation kit (System Biosciences) was used to isolate OMVs, with slight modifications to the manufacturer's protocol. Briefly, cells were spun down (10 min, 4000 × g, 4°C) and the supernatant was transferred to a new tube and centrifuged again. The supernatant was then filtered through a 0.45-μm sterile filter. The additional filtration step through a 0.2-μm filter was omitted to preserve OMVs, which may be ~200 nm in diameter (Kulp and Kuehn 2010). Column preparation, OMV capture, and elution were performed according to the manufacturer's instructions. Fresh LB was subjected to the purification process to obtain a buffer control. Isolated OMVs were analyzed by SDS-PAGE and SYPRO™ Orange total protein staining according to the manufacturer's instructions.

For LPS quantification, isolated OMVs were analyzed by SDS-PAGE, and biomolecules were transferred to a nitrocellulose membrane using the Trans-Blot® Turbo™ Transfer System (Bio-Rad) and consumables. After a 5-min blocking step in EveryBlot blocking buffer (Bio-Rad), the mouse antilipopolysaccharide core monoclonal antibody mAb WN1 222–5 (Hycult Biotech) was added at a dilution of 1:4000 and incubated for 1 h at RT. The membrane was rinsed three times with TBST and washed four times in TBST for 5 min each. StarBright Blue 700 Goat Anti-Mouse IgG (Bio-Rad) was then diluted 1:2500 in EveryBlot blocking buffer and incubated with the membrane for 1 h. After repeated rinses and washes, the membrane was dried, and the fluorescence signal was detected using a ChemiDoc™ MP (Bio-Rad). Analysis was performed with ImageLab software (Bio-Rad).

Cryoscanning electron microscopy

Bacteria were cultured as described for growth curve analysis. After 18 h of growth, cells were washed three times in ddH$_2$O (Roth), concentrated three times, and 1.5 μl of the cell suspension was spotted on a piece of potato dextrose (PD) agar mounted on a carrier. The sample volume for isolated OMVs was 2 μl. The carrier was inserted into slush nitrogen for rapid freezing and then transferred to the cryochamber. Sublimation conditions were 20 min or 30 min at −90°C for whole cells and isolated OMVs, respectively. Platinum coating was applied at 15 mA for 180 s, and imaging was performed at 3 or 5 kV.

Protein purification

Protein overproduction for analytical protein purification was induced at an OD_{600} of ~0.6–0.8 by adding 1 mM isopropyl-β-D-1-thiogalactopyranoside (IPTG) or 200 ng/ml AHT and incubation at 30°C (shaking) for 3 h unless otherwise stated. Cells from a 333 ml culture were harvested by centrifugation (10 min, 4000 × g, 4°C) and washed in 20 mM HEPES pH 8.0. Cell pellets were stored at −20°C. Cell lysis was performed according to the instructions for BugBuster® Master Mix (Novagen) supplemented with 1 × cOmplete™ EDTA-free protease inhibitor cocktail (Roche) or by three passages through a French press mini cell at 900 psi in the indicated lysis buffer. The lysate was cleared by centrifugation (≥ 20 min, 16 000 × g, 4°C) and used for protein purification.

Protein purification of [His]SAS1 from *Bacillus subtilis*

Escherichia coli BL21 (DE3) harboring pET24d::*his$_6$-SAS1* was grown at 37°C until it reached an OD_{600} of ~0.6–0.8 and was induced by adding 12.5 g/l D(+)-lactose monohydrate (Sigma). After 20 h at 30°C, cells were harvested as described. The cell pellet was resuspended in 10 ml of wash buffer [20 mM HEPES/NaOH (pH 8.0), 250 mM NaCl, 40 mM imidazole, 20 mM MgCl$_2$, 20 mM KCl], supplemented 0.1 mg/ml of DNase I, RNase A, lysozyme, and 1 × cOmplete™ EDTA-free protease inhibitor cocktail (Roche). Cells were lysed by three passages through a French press mini cell at 900 psi. The cleared lysate was applied to 1 ml of equilibrated nickel nitrilotriacetic acid (Ni-NTA) agarose (Qiagen) and washed three times with 10 ml of wash buffer. [His]SAS1 was eluted by adding 1 ml of elution buffer [20 mM HEPES/NaOH (pH 8.0), 250 mM NaCl, 500 mM imidazole, 20 mM MgCl$_2$, 20 mM KCl] five times. [His]SAS1 was buffer exchanged in storage buffer [20 mM HEPES/NaOH (pH 7.5), 200 mM NaCl, 20 mM MgCl$_2$, 20 mM KCl] and concentrated using a 30 kDa Amicon® (Millipore). Protein concentration was determined using the Roti®-Quant reagent (Carl Roth) using BSA as a standard, and the aliquots were stored at −80°C.

Synthesis of ppGpp

To prepare cold or P32-labeled ppGpp (200 μl reaction), 5 μM [His]SAS1 was incubated with 5 mM cold ATP or 100 μCi (3.7 Mbq) [P32]ATP and 5 mM GDP in reaction buffer [100 mM HEPES/NaOH (pH 7.5), 200 mM NaCl, 20 mM MgCl$_2$, 20 mM KCl]. After 3 h at 37°C, SAS1 was precipitated by adding one volume of chloroform and vortexing for 10 s. The solution was centrifuged (5 min, 16 000 × g, 4°C), and the upper aqueous phase was transferred to a new 2 ml reaction tube. Nucleotides were precipitated by adding one volume of 2 M LiCl. In total, four volumes of 100% ice-cold EtOH were added, and the reaction tube was incubated at −20°C for 20 min. After centrifugation (20 min, 16 000 × g, 4°C), the supernatant was removed, and the pellet was air-dried. The pellet was resuspended in 100 μl of binding buffer [10 mM Tris/HCl (pH 8.0), 100 mM NaCl, 5 mM MgCl$_2$]. The quality of the ppGpp preparation was checked by PEI-cellulose thin-layer chromatography (TLC) developed for 3 h in 1.5 M KH$_2$PO$_4$ (Corrigan et al. 2016). After exposure of the TLC plate to a phosphor screen (Cytiva), signals were detected using a Typhoon™ laser scanner (Cytiva). The conversion of [P32]ATP to [P32]ppGpp was 91%.

High-performance liquid chromatography (HPLC)-purified ppGpp × 6 Li$^+$ and pppGpp × 7 Li$^+$ (Li$^+$ refers to lithium ions originating the precipitation step with LiCl) were produced as described in (Steinchen et al. 2015) with minor modifications. In brief, 5 μM *Bacillus subtilis* SAS1 was incubated with 5 mM ATP and

5 mM GDP or GTP in buffer (100 mM of HEPES-Na, pH 7.5, 250 mM NaCl, 20 mM MgCl2, 20 mM KCl) for 30 min at 37°C. Thereafter, SAS1 was precipitated by addition of one volume part of chloroform. The aqueous phase that contained the nucleotides was diluted with double-distilled water to a total volume of 5 ml and subjected to anion exchange chromatography (ResourceQ, 6-ml; GE Healthcare) and nucleotides eluted with a gradient of LiCl. The products ppGpp and pppGpp were precipitated by adding lithium chloride to a final concentration of 1 M, followed by adding four volumes of ethanol. The suspension was incubated on ice for 20 min and centrifuged (20 min, 5000 × g, 4°C). The resulting pellets were washed multiple times with absolute ethanol, dried, and stored at −20°C. The quality of the so-prepared ppGpp and pppGpp was controlled by analytical HPLC.

Differential radial capillary action of ligand assay

A 96-well plate containing 200 μl LB + Cm per well was inoculated with the respective ASKA strains. The plate was incubated overnight at 30°C without shaking. In a Nunc™ 2 ml 96-DeepWell™ plate (Thermo Scientific™), 1 ml LB + Cm per well was inoculated by adding the overnight culture at a 1:50 dilution. The plate was sealed with Breathe-Easy®, and the cultures were allowed to grow at 37°C for 3 h. Protein overproduction was induced by adding 1 mM IPTG and incubating at 30°C for 3 h. The plate was centrifuged (10 min, 2000 × g, 4°C), and the supernatant was discarded. Cells were resuspended in 60 μl lysis buffer per well (250 μg/ml lysozyme, 10 μg/ml DNase I, and 1 × cOmplete™ EDTA-free in binding buffer) by shaking for 10 min at RT. Cells were subjected to two freeze–thaw cycles (30 min at −80°C and 30 min at RT), and the plates were stored at −80°C until further use. [P32]ppGpp was diluted 1:400 in binding buffer. A volume of 20 μl of this solution was added to each well (mixed by gentle shaking for 2 min), and 2 μl/well was transferred to a nitrocellulose membrane using a 96-well pin tool. The membrane was dried at RT and placed on a phosphor screen for 12–24 h. Signals were detected using a Typhoon™ laser scanner (Cytiva Europe). [His]RelA and empty vector (EV) controls were included in each plate. The relative binding of ppGpp in each plate was normalized to [His]RelA (100%).

Purification of [strep]LpxA, [strep]RnhB, and [strep]RnhB

W3110 Δ*relA*Δ*spoT* cells ((p)ppGpp⁰) were used for the overproduction of [strep]LpxA, [strep]RnhB, and [strep]RnhA to avoid contamination of (p)ppGpp in protein preparations. Cells were lysed in BugBuster® Master Mix (Novagen) supplemented with 1 × cOmplete™ EDTA-free protease inhibitor (Roche) according to the manufacturer's instructions. Purification was performed using the Strep-Tactin® Sepharose® (IBA Lifesciences) strep-tag purification kit.

Purification of V. *harveyi* AasS[His]

Cell pellets from 1 l of bacterial culture were resuspended in 10 ml of lysis buffer [20 mM HEPES/NaOH (pH 8.0), 500 mM NaCl, 10% (v/v) glycerol, 10 mM imidazole, 1 × cOmplete™ EDTA-free; 0.1 mg/ml of lysozyme, DNase I, RNase A] and lysed by French press. The cleared lysate was applied to a pre-equilibrated Ni-NTA agarose column (Qiagen) and allowed to flow through. After three 10-column volumes (CV) wash steps with wash buffers I–III [20 mM HEPES/NaOH (pH 8.0), 500/300/150 mM NaCl (I/II/III), 10% (v/v) glycerol, 50 mM imidazole], AasS[His] was eluted in wash buffer III supplemented with 250 mM imidazole. Through a PD-10 gravity-flow column, AasS[His] was buffered in 20 mM Tris-

HCl (pH 7.5), 10% (v/v) glycerol, 1 mM EDTA, 0.1 mM tris-(2-carboxyethyl)phosphine (TCEP), and 0.002% (v/v) Triton X-100 for storage at −80°C as previously described (Jiang et al. 2006). Protein concentration was determined using the Roti®-Quant reagent (Carl Roth) using BSA as a standard.

Biosynthesis and purification of acyl-ACP

Holo-ACP was produced according to (Jenkins and Dotson 2012) with minor modifications. BL21 (DE3), carrying pACYCDuet-1::*acpS*[his] + *acpP*, was induced with 1 mM IPTG and grown overnight at 18°C to allow simultaneous overproduction of AcpS[His] and AcpP. Cell pellets from 1 l of bacterial culture were resuspended in 10 ml buffer A [20 mM HEPES/NaOH (pH 8.0), 1 mM TCEP (pH 7.0)], which was supplemented with 0.1 mg/ml of lysozyme, DNase I, and RNase A. After French press-mediated cell lysis, the cleared lysate was applied to a Ni-NTA gravity-flow column (Qiagen) pre-equilibrated with buffer A. The resin was washed twice with five CVs of buffer A. AcpS[His] was eluted by applying an imidazole gradient (10–1000 mM). The 50–1000-mM imidazole elution fractions were pooled, and an equal volume of ice-cold isopropanol was added slowly with gentle stirring at 4°C. After 1 h at 4°C, aggregated proteins were removed by centrifugation (30 min, 16 000 × g, 4°C), and an equal volume of buffer A was added. The solution was injected into an AEKTA Superloop™ and automatically applied to a HiScreen™ QHP column (4.7 ml CV; Cytiva) equilibrated with buffer A. After washing with five CVs buffer A, an 80 ml linear gradient of NaCl (0–500 mM) in buffer A was applied to elute holo-ACP. Holo-ACP eluted at ∼300 mM NaCl, and the fractions were analyzed by SDS-PAGE, Coomassie, and SYPRO™ Orange staining (Sigma). AcpP was only visible on SYPRO™ Orange stained SDS-PAGE. AcpP-containing fractions were pooled, buffer exchanged, and concentrated in 20 mM HEPES/NaOH (pH 8.0) using an Amicon® with a 3-kDa cutoff. Protein concentration was determined with the Pierce™ BCA protein assay kit (Thermo Scientific™) using BSA as a standard. Holo-ACP was reduced in the presence of two molar equivalents of TCEP (pH 7.0) for 1 h at RT. Holo-ACP was acylated in a 10 ml reaction containing 23 μM reduced holo-ACP, 100 mM Tris/HCl (pH 7.5), 5 mM ATP, 5 mM MgCl2, 100 μm TCEP (pH 7.0), 0.01% (v/v) Triton X-100, 100 μg AasS[His] and 300 μM R-3-hydroxymyristic acid. The reaction was incubated for 45 min at 30°C, after which 50 μg of AasS[His] was added again, followed by 20 min at 30°C. The reaction mixture was cooled and applied directly to a HiScreen™ QHP column (4.7 ml CV; Cytiva), pre-equilibrated in 20 mM HEPES/NaOH (pH 8.0). After a three-CV wash, an 80 ml linear NaCl gradient (0–500 mM) was applied, and acyl-ACP was eluted at around 300 mM NaCl. Acylation was confirmed by SDS-PAGE and SYPRO™ Orange staining, as acyl-ACP migrated faster through the gel matrix. Since it was not possible to separate holo- and acyl-ACP, the acyl-ACP containing fractions were pooled, buffer exchanged, and concentrated in 20 mM HEPES/NaOH (pH 7.0) via an Amicon® with a 3-kDa cutoff. A molar excess of N-ethylmaleimide (NEM; Sigma) was added to block free thiol groups from remaining holo-ACP. After 2 h at RT and 16 h at 4°C, NEM was removed by buffer exchange in 20 mM HEPES/NaOH (pH 7.0). The NEM-blocked acyl-ACP preparation was then buffer exchanged and concentrated in 20 mM HEPES/NaOH (pH 8.0). SDS-PAGE and SYPRO™ Orange staining was used to visualize and determine the relative band intensity of acyl-ACP. Protein concentration was determined via BCA assay with BSA as a standard and adjusted to the relative amount of acyl-ACP. This acyl-ACP preparation was stored at −20°C until further use.

Synthesis and purification of a ThioGlo–ACP conjugate

The conjugation of ThioGlo®1 and holo-ACP was performed as previously described with minor modifications (Jenkins and Dotson 2012). Briefly, in a 1 ml reaction, 100 µM holo-ACP, 1 mM TCEP, and 132 µM ThioGlo®, 20 mM HEPES/NaOH (pH 8.0), 5% (v/v) dimethyl sulfoxide (DMSO) was incubated for 25 min at 25°C. An additional 132 µM ThioGlo® was added and incubated for 35 min. The conjugate was buffer exchanged in 20 mM HEPES/NaOH (pH 8.0) using a PD-10 gravity-flow column. Protein concentrations were determined via Pierce™ BCA protein assay kit using BSA as a standard.

Fluorescent LpxA activity assay

The assay was performed at 25°C in black 96-well half-area plates (Corning). All components were diluted in 20 mM HEPES/NaOH (pH 8.0). For a typical reaction, 10 µl 20 mM HEPES (pH 8.0), 20 µl of 53.85 µM NEM-blocked acyl-ACP preparation (with acyl-ACP making up 14.68 µM of the preparation as determined by densitometric analysis), 20 µl of UDP-GlcNAc (various concentrations), 30 µl of 33.333 µM ThioGlo® 1, and 10 µl of (p)ppGpp or LiCl buffer control were mixed. The plate was equilibrated in a Tecan Infinite® M Plex in the dark at 25°C for 5 min. Then 10 µl of 100 nM ^{strep}LpxA (calculated as a monomer; or buffer for the no-enzyme control) were added. The reaction was mixed by pipetting up and down, and the fluorescence intensity was monitored for 10 min at λ_{ex} = 379 nm and λ_{em} = 513 nm at 10 s intervals. LpxA was diluted fresh before each run. A typical reaction to determine IC_{50} values consisted of 20 µl of 13.46 µM acyl-ACP preparation (with acyl-ACP making up 3.67 µM), 20 µl of 20 mM UDP-GlcNAc, 30 µl of 33.333 µM ThioGlo®, 20 µl of nucleotide (various concentrations) and was started by adding 10 µl of 100 nM ^{strep}LpxA. The nucleotide dilutions were set up in the respective LiCl control buffer.

An independent batch of acyl-ACP was used to assess the effect of other proteins on the activity of ^{strep}LpxA. A typical reaction contained 10 µl of 20 mM HEPES (pH 8.0), 20 µl of acyl-ACP (35.79 µM with acyl-ACP making up 12.13 µM), 20 µl of 20 mM UDP-GlcNAc and 30 µl of 33.333 µM ThioGlo® 1. The plate was equilibrated in a Tecan Infinite® M Plex for 5 min at 25°C in the dark. 50 nM ^{strep}LpxA was incubated with various concentrations of protein ligands (up to 5 µM) in a 96-well plate at RT for 30 min with gentle shaking. 20 µl of this protein solution was added to the equilibrated master mix to start the reaction. A control reaction containing no protein–ligand was used to normalize LpxA activity to 100%. In another control reaction, LpxA was omitted to check the highest protein–ligand concentration for background activity.

Thermal shift assay

A typical 25 µl reaction was composed of 20 µl purified protein at a maximum concentration of 1 mg/ml, 2 µl of ppGpp (nonpurified preparation) or 10 mM nucleotide solution in binding buffer [10 mM Tris/HCl (pH 8.0), 100 mM NaCl, 5 mM MgCl$_2$] and 3 µl 83.33 × SYPRO™ Orange. All components were pipetted on ice, and the PCR plate was sealed with an adhesive film and flicked to mix the content. After brief centrifugation (1 min, 500 × *g*, 4°C), the plate was transferred to a CFX Connect™ real-time PCR detection system (Bio-Rad). After 2 min at 25°C, a temperature gradient was applied from 25°C to 95°C in increments of 0.5°C. Each temperature was held for 10 s, and the relative fluorescence intensity was measured in the FRET channel. CFX Maestro™ (Bio-Rad) and OriginPro 2020 were used for data analysis and visualization.

Continuous fluorescent RNase H activity assay

RNase H activity was monitored in 100 µl reactions with final concentrations of 50 mM Tris/HCl (pH 8.0), 5.8 mM MgCl$_2$, 1 mM DTT, 60 mM KCl, 200 nM RNase HII (calculated as a monomer), and 0.5 µM of the molecular beacon. The buffer composition was adapted from the protocol described by Corona and Tramontano (2015). The molecular beacon was described by Rizzo et al. (2002). Reagents that omitted the molecular beacon were joined in the well of a black 96-well half-area plate (Corning). To determine the effect of nucleotides on RnhB, 2-fold serial dilutions of ATP, GTP, GDP, or ppGpp were prepared in LiCl buffer (same concentration as in the ppGpp preparation) to exclude buffer effects. The serial dilutions were added to the mastermix. The plate was pre-equilibrated in a Tecan Infinite® M Plex microplate reader at 37°C for 10 min. The reaction was started by adding the molecular beacon and then mixed by pipetting. The fluorescence intensity was monitored for 1 h at 37°C with continuous measurements at λ_{ex} = 490 nm and λ_{em} = 540 nm. Note that the molecular beacon had to be diluted fresh before each measurement to generate stable results. RNase H activity was calculated based on a standard curve of the fully digested molecular beacon. For that, 1.66 µM molecular beacon was incubated with 5 U of RNase HI (New England Biolabs) at 37°C for 18 h in the reaction buffer mentioned. RNase H activity was calculated from the initial velocity.

Microscale thermophoresis

Protein–protein interactions were investigated by MST. Since ^{His}RnhB and ^{His}RnhA were not particularly thermally stable in 20 mM HEPES pH 8, we sought to stabilize buffer conditions to avoid infrared laser-induced aggregation of the proteins. MST experiments with these two proteins were fluorescently labeled in buffer M [20 mM HEPES/NaOH (pH 8.0), 2.5% (v/v) glycerol, 1.5 µM BSA, 5 mM MgCl$_2$, 50 mM NaCl] according to the manufacturer's instructions for the His-Tag Labeling Kit RED-tris-NTA (NanoTemper Technologies GmbH). A total of 50 nM labeled protein was incubated with serial dilutions of ^{strep}LpxA (diluted in 20 mM HEPES pH 8). In the case of $^{His-SUMO}$RnhB or $^{His-SUMO}$RnhA, labeling could be performed in the manufacturer's recommended PBS-T buffer, and 50 nM labeled protein was incubated with serial dilutions of ^{strep}LpxA (diluted in 20 mM HEPES pH 8). MST experiments were performed with medium laser intensity and autosensitivity and analyzed with MO.Affinity analysis software.

Results

Do LPS biosynthesis enzymes bind (p)ppGpp?

The biosynthesis of PL and peptidoglycan (PGN) in *E. coli* are regulated by (p)ppGpp (Stein and Bloch 1976, Ramey and Ishiguro 1978). These findings raise the question of whether LPS biosynthesis is also subject to this control since all three pathways diverge from similar precursors (Fig. 1B). Intriguingly, previous studies provided evidence for a contribution of (p)ppGpp in the regulation of LPS biosynthesis (Schäkermann et al. 2013, Roghanian et al. 2019, Thomanek et al. 2019). Hence, we asked whether enzymes catalyzing early steps of lipid A biosynthesis bind the nucleotide and used the differential radial capillary action of ligand assay (DRaCALA) with cell lysates of the ASKA overexpression collection and radio-labeled ppGpp. An EV-carrying strain was the negative control, and RelA represented the positive control (Fig. 2A). Relative to RelA (100%), the previously confirmed ppGpp binders InfB, ObgE, and SpeF scored 97 ± 11%, 86 ± 12%, and 73 ± 12%, respectively, relative to RelA (Fig. 2B).
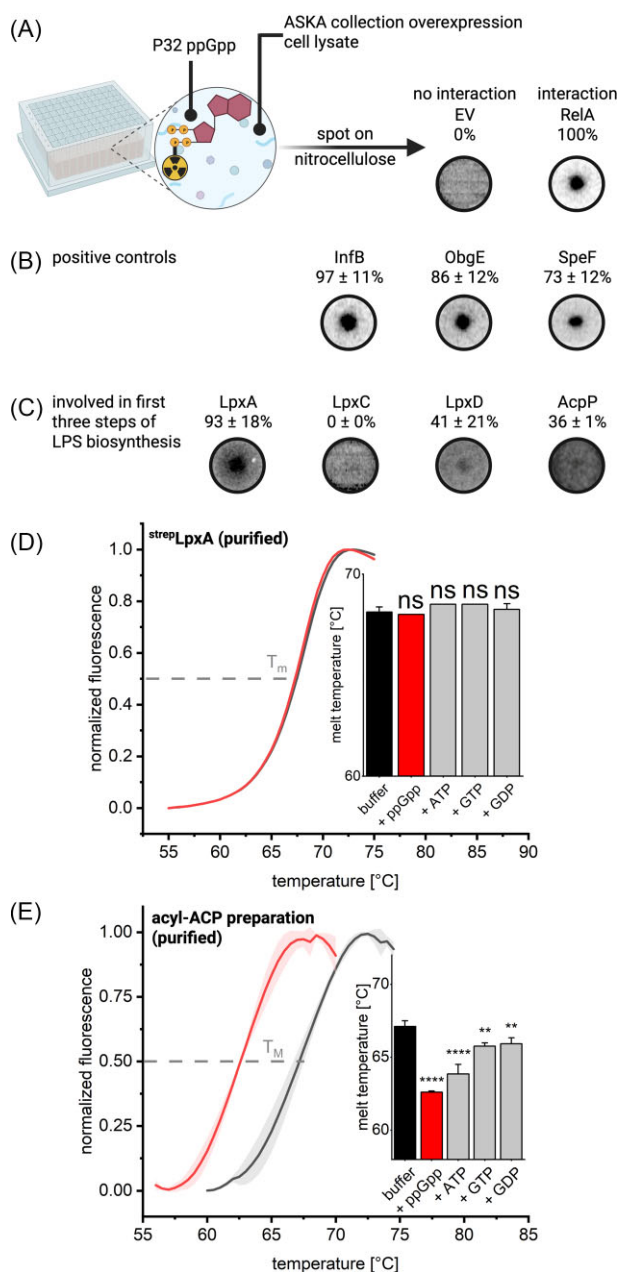
Figure 2. Assessment of ppGpp-binding to key proteins of the LPS biosynthesis pathway. **(A)** Schematic representation of DRaCALA experiments. The ASKA collection was used for high-throughput individual overexpression of *E. coli* genes. Crude cell lysates were incubated with radio-labeled ppGpp and stamped onto nitrocellulose membranes. Binding of ppGpp to a protein resulted in a distinct spot that was quantified relative to [His]RelA (100%). **(B)** Positive controls for DRaCALA experiments included previously identified ppGpp-binding proteins. **(C)** Proteins involved in the first three steps of LPS biosynthesis were analyzed for ppGpp-binding using DRaCALA experiments. The *acpP* gene encodes the apo form of ACP, whose activated and acylated form acts as a fatty acid donor for LpxA and LpxD. **(D)** Purified [strep]LpxA was analyzed by thermal shift assays to generate melting curves of the protein in the presence of buffer or ligands. The curve represents the Boltzmann fit to the melting curves of four technical replicates; error bars represent the standard deviation (SD). The bar graph visualizes the mean melting temperatures of the protein in the presence of different ligands; error bars represent the SD. Ns: not significant when $P > .5$ or when the temperature shift was $\leq 1°C$ compared to protein in buffer. **(E)** As in (D), but an acyl-ACP preparation was analyzed with thermal shift assays.

Next, we examined the enzymes responsible for the first three steps of lipid A biosynthesis, namely LpxA, LpxC, and LpxD, as well as the acyl donor acyl-ACP utilized by LpxA and LpxD, for ppGpp binding. Note that the *acpP* construct encodes the inactive apo-form of the acyl carrier protein. AcpS is required to add a 4'-phosphopantetheine to apo-ACP post-translationally. The resulting holo-ACP is the physiologically active form and can be loaded with an acyl chain (Flugel et al. 2000).

Although cellular LpxC levels are controlled by (p)ppGpp in a growth phase-dependent manner (Schäkermann et al. 2013), LpxC itself does not seem to bind ppGpp (Fig. 2C). In contrast, the lysate of the *lpxA* overexpression strain appeared to bind the nucleotide (93 ± 18% relative to RelA). The *lpxD* and *acpP* strains showed intermediate binding of 41% ± 21%, and 36% ± 1%, respectively. LpxA, thus emerged as a putative ppGpp-binding protein.

Since cell lysates contain a wide variety of components, we purified [strep]LpxA from the (p)ppGpp[0] strain (to prevent carryover of (p)ppGpp) and examined it by the thermal shift assay. In this assay, the recombinant protein is subjected to a stepwise increase in temperature in the presence of the fluorescent dye SYPRO™ Orange in a real-time PCR cycler. Thermal melting of the protein results in binding of the dye to liberated hydrophobic regions and a fluorescent signal. The binding of a ligand typically shifts the melting curve to the right or left. For LpxA, no significant shift (>1°C) was detected in response to nucleotides ppGpp, ATP, GTP, or GDP (Fig. 2D). This result was confirmed by isothermal titration calorimetry (ITC; data not shown). In contrast, a substantial shift towards lower temperatures was observed for ppGpp and other nucleotides with an acyl-ACP preparation, which contained a mixture of NEM-blocked holo-ACP and *R*-3-hydroxymyristoyl-ACP (Fig. 2E). The apparent binding of ppGpp to LpxA in cell lysates, but the absence of ppGpp binding with purified LpxA suggests that some cellular factor in the lysate mediates that apparent binding. The most likely candidate is AcpP.

(p)ppGpp inhibits LpxA activity *in vitro*, likely through interaction with acyl-ACP

The findings described above, raised the possibility that (p)ppGpp affects the first step of lipid A biosynthesis. To address whether (p)ppGpp influences the LpxA-catalyzed reaction, we set up a continuous fluorescent activity assay (Jenkins and Dotson 2012). LpxA catalyzes the transfer of the acyl group from acyl-ACP to UDP-GlcNAc, liberating a thiol group on ACP (holo-ACP; Fig. 3A). The ThioGlo1 dye can conjugate with the liberated thiol group to generate a fluorescent signal (Fig. 3B). We determined the Michaelis–Menten kinetics of the LpxA reaction in the presence and absence of ppGpp. A total of 800 μM ppGpp (found intracellularly during the stringent response; Varik et al. 2017) had an inhibitory effect on LpxA activity ($V_{max} = 199 \pm 5$ pmol∗min[-1]; $K_m = 539 \pm 46$ μM) compared to the LiCl-containing buffer control ($V_{max} = 291 \pm 8$ pmol∗min[-1]; $K_m = 494 \pm 51$ μM) (Fig. 3C). A very similar inhibitory effect was observed with 800 μM of pppGpp ($V_{max} = 127 \pm 9$ pmol∗min[-1]; $K_m = 967 \pm 187$ μM) compared to the buffer control ($V_{max} = 195 \pm 15$ pmol∗min[-1]; $K_m = 600 \pm 152$ μM). On the contrary, 800 μM CTP did not have an inhibitory effect on the reaction ($V_{max} = 187 \pm 10$ pmol∗min[-1]; $K_m = 501 \pm 98$ μM).

The addition of increasing concentrations of (p)ppGpp to the LpxA assay revealed a dose–response effect, supporting a function as an inhibitor (Fig. 3E and F). Note that the final concentrations of acyl-ACP in these experiments were lower (2.69 μM) than in the Michaelis–Menten experiments (10.77 μM) to save the scarce acyl-ACP. Under these conditions, ppGpp and pppGpp showed
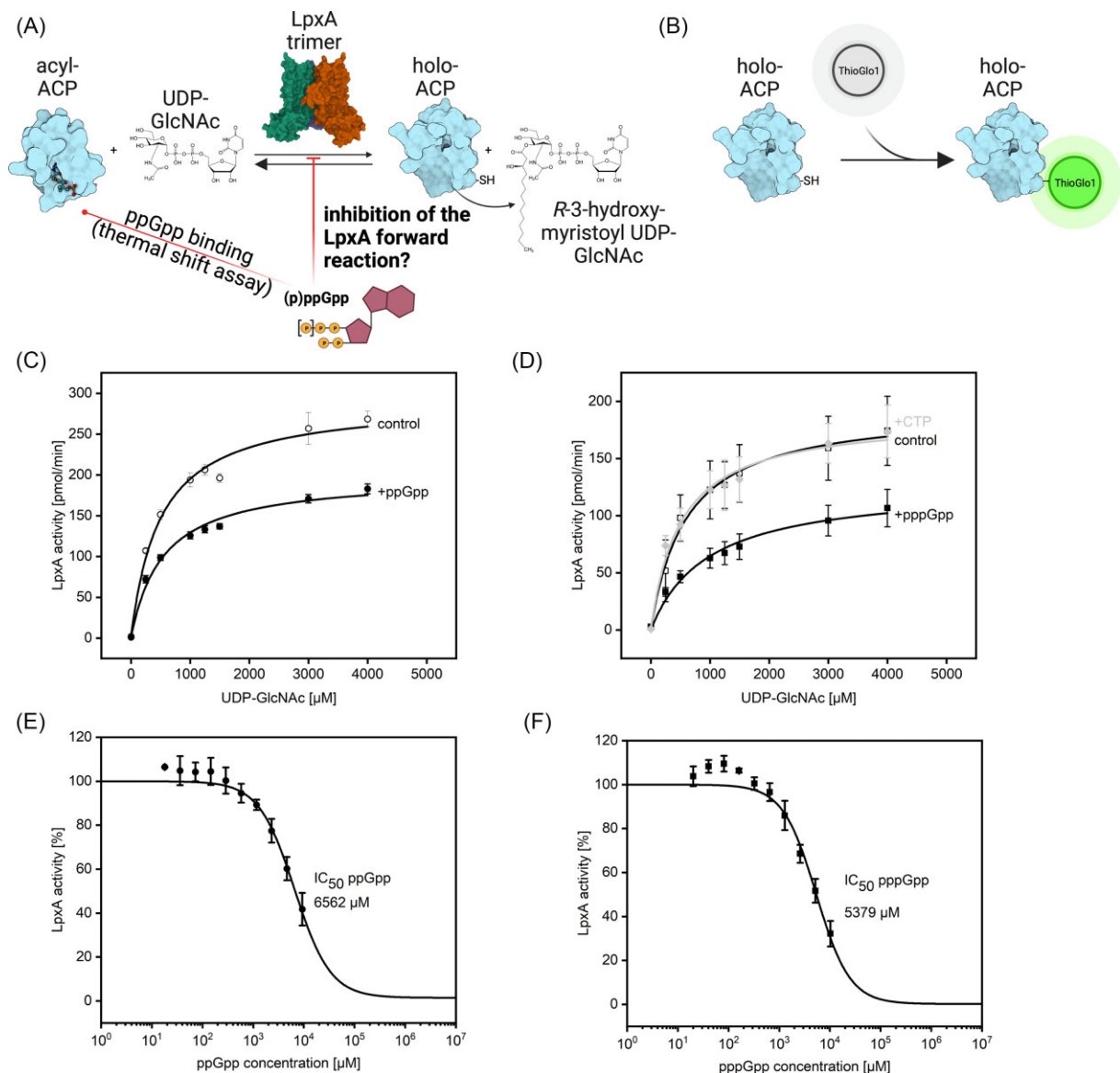
Figure 3. LpxA catalyzes the first step in the biosynthesis of LPS and is inhibited by (p)ppGpp. **(A)** LpxA uses acyl-ACP and UDP-GlcNAc as substrates and transfers the fatty acid chain to generate R-3-myristoyl-UDP-GlcNAc. This process liberates a thiol group on ACP (holo-ACP). PDB codes for visualization: 1LXA (LpxA; Raetz and Roderick 1995, Roderick 1995), 2FAC (acyl-ACP; Roujeinikova 2006, Roujeinikova et al. 2007), and 1ACP (holo-ACP; Kim and Prestegard 1990, Prestegard and Kim 1993). **(B)** The fluorescent dye ThioGlo1 included in the LpxA assay reaction mixture can rapidly conjugate with the free thiol group and generate a fluorescent signal. **(C)** and **(D)** Michaelis–Menten plots for LpxA activity in the presence of ppGpp-LiCl control buffer or 800 μM ppGpp or pppGpp-LiCl control buffer, 800 μM pppGpp or 800 μM CTP. The line represents a fit to the Michaelis–Menten equation and combines three technical replicates, where the points with error bars represent the mean values and SD. The UDP-GlcNAc concentration was varied. **(E)** and **(F)** Dose–response experiments in which the substrate and enzyme concentrations were kept constant, but the concentrations of ppGpp and pppGpp were varied, respectively. Serial dilutions of nucleotides were performed in the corresponding LiCl control buffer to exclude buffer effects. The line represents a logistic fit and combines three technical replicates. The upper and lower limits were determined empirically (LpxA alone and no LpxA, respectively). Data points with error bars represent the mean and SD.

inhibitory effects only at higher concentrations (IC50 ppGpp = 6562 ± 472 μM; IC50 pppGpp = 5379 ± 399 μM). Reactions without (p)ppGpp (= 100%) or without LpxA empirically determined the fit limits. Cumulatively, these results suggest that ppGpp and pppGpp can inhibit the first step of lipid A biosynthesis *in vitro*.

Overexpression of *lpxA* and the absence of (p)ppGpp increases cell length

To establish a link between LpxA and (p)ppGpp *in vivo*, we over-produced plasmid-encoded [strep]LpxA in a Δ*relA*Δ*spoT* [(p)ppGpp⁰] mutant or the isogenic W3110 WT strain and monitored growth

in 96-well plates (Fig. 4A and B). Consistent with a previous report (Guo et al. 2022), we did not detect any obvious growth defects. We went a step further and determined cell viability at the end of the growth curve using the resazurin assay, which is based on the intracellular reduction of the nonfluorescent dye resazurin to highly fluorescent resorufin by metabolically active cells. Reduced metabolic activity or altered redox potential of cells results in lower conversion of resazurin. Here, we noticed that the WT had lower viability after overproduction of [strep]LpxA (62 ± 8%; P = .0118), while the viability of the (p)ppGpp⁰ strain was barely affected (93 ± 3%; P = .0984) suggesting that the mutant does not respond equally to excess LpxA. Cultures were also serially diluted
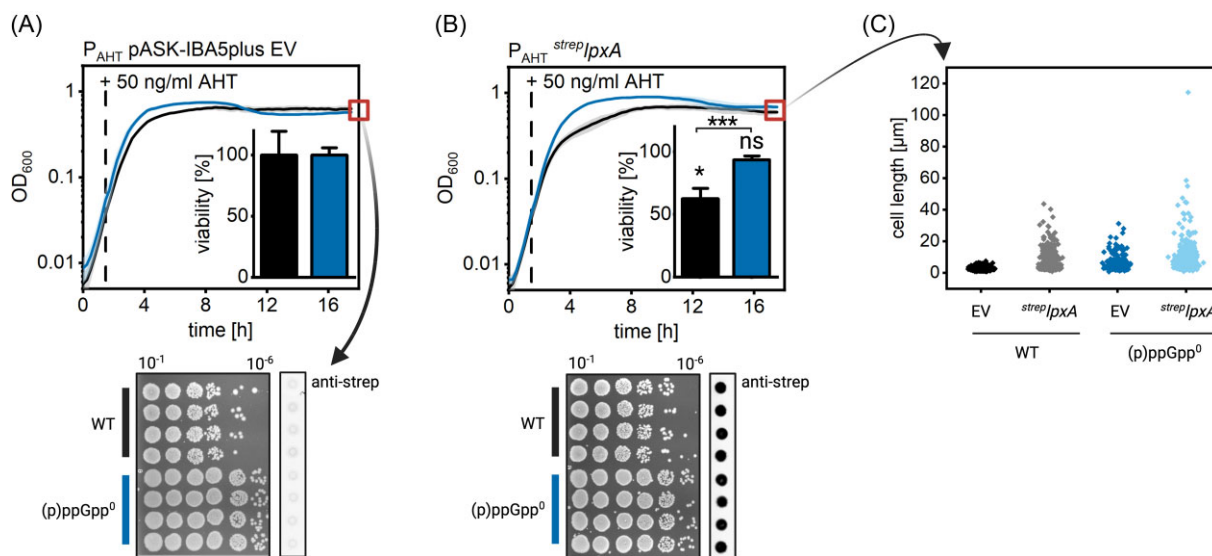
Figure 4. Effect of of ^{strep}lpxA overexpression on growth, viability and cell length. **(A)** Growth curves of W3110 WT (black) and (p)ppGpp^0 (blue) harboring the EV. The line represents the mean of four biological replicates, and the error band represents the standard deviation (SD). Overexpression was induced by adding 50 ng/ml AHT after 105 min of growth. Cell viability was measured after overnight cultivation using the resazurin assay (bar graph) and normalized for each strain carrying the EV. Cells after overnight cultivation were also serially diluted and spotted on LB agar to determine CFU. Crude cell lysates were spotted onto a nitrocellulose membrane and subjected to dot-blot analysis to detect strep-tagged proteins. **(B)** As in (A), but ^{strep}lpxA was overexpressed. **(C)** Overnight overexpression cultures were subjected to microscopy to quantify cell lengths.

and spotted on LB agar to determine colony-forming units (CFU). The (p)ppGpp^0 mutant generally reached higher CFU counts at the same final OD_{600}. Overproduction of ^{strep}LpxA to comparable levels had no apparent effect on CFU counts in both strains.

To obtain clues as to whether *E. coli* changes its cell shape when LpxA and/or (p)ppGpp concentrations are high, we examined stationary cells under the microscope (Fig. 4C; Table S4, Supporting Information). Compared to the WT harboring the EV, we observed massive cell elongation in response to ^{strep}LpxA overproduction (Figure S1, Supporting Information). The (p)ppGpp^0 strain with EV already had elongated cells of similar length, which increased further in response to ^{strep}LpxA production (Figure S2, Supporting Information). Cumulatively, these results support a role of (p)ppGpp in maintaining cell envelope homeostasis.

Overexpression of *lpxA* and/or the absence of (p)ppGpp elicit OMV formation

PGN determines the cell shape because of its rigidity (Silhavy et al. 2010). It has been reported that the accumulation of PGN fragments, or LPS, or an altered fatty acid composition can affect the formation of OMVs, which are 20–250 nm in diameter (Schwechheimer and Kuehn 2015, McMillan and Kuehn 2021) (Fig. 5A). To assess whether the overproduction of ^{strep}LpxA or the absence of (p)ppGpp affect OMV formation, we isolated OMVs from cell-free culture supernatant using the ExoBacteria™ OMV isolation kit. The isolated OMVs could be visualized by cryo-SEM (Fig. 5B) and were ~200 nm in diameter. The examination of entire cells by cryo-SEM supported the elongation of ^{strep}LpxA overproducing cells (compare Fig. 4C) and revealed an abundant vesiculation of OMVs in the (p)ppGpp^0 mutant (Fig. 5C; examples of all four strains shown in Figure S3, Supporting Information). The visible vesiculation from intact cells, in combination with the unchanged CFU counts (Fig. 4A and B), indicated that the OMVs were not a result of spontaneous cell lysis.

The isolated OMVs were analyzed for their protein and LPS content. Proteins were visualized by SDS-PAGE and staining with the sensitive SYPRO™ Orange dye (detection limit: 4–8 protein/band) (Fig. 5D and E). Overproduction of ^{strep}LpxA resulted in three times more OMV-associated proteins in the WT compared to the same strain with EV ($P = .0014$). The (p)ppGpp^0 mutant had 10 times more OMV-associated proteins ($P = .0136$) and 24 times more after ^{strep}LpxA overproduction ($P = .0010$) than the corresponding WT strains. The LPS content was visualized after SDS-PAGE by immunoblotting with an anti core-LPS antibody (Fig. 5F). Commercially available LPS (from *E. coli* O111: B4, Sigma-Aldrich) was used for quantification. Increased LPS levels were found in the OMV preparations from the (p)ppGpp^0 mutant generally, but in both strains, LPS levels remained largely unaffected by the overproduction of ^{strep}LpxA. In relative terms, and somewhat unexpectedly, the level of LPS decreased in response to ^{strep}LpxA overproduction (Fig. 5G). The reduced LPS/protein ratio is probably explained by the thermodynamically unfavorable forward reaction and the preferred reverse reaction that LpxA is catalyzing (Fig. 1B) (Anderson et al. 1993).

The overproduction of RnhB results in elongated cells and OMV formation

Given that LpxA altered the cell length and OMV formation, we decided to assay other genes involved in cell envelope biosynthesis by similar experiments. Production of the proteins was confirmed by western blot analysis (data not shown). While ^{strep}LpxC and ^{strep}LpxD barely affected cell length, ^{strep}LpxA almost doubled the average cell length (Fig. 6A and Table S4, Supporting Information; compilation of representative microscopy images in Figures S1 and S2, Supporting Information). As an organism–foreign control protein, we used ^{strep}mCherry, which also triggered some cell elongation but clearly much less than ^{strep}LpxA. FabZ and MurA catalyze the first steps of PL and PGN biosynthesis, respectively (Fig. 1B). In the WT strain, ^{strep}FabZ or ^{strep}MurA production barely affected cell length (Table S4, Supporting Information).

The *lpxA* gene is organized in an operon along with *fabZ*, *lpxD*, *lpxB*, and other genes like *rnhB*. As the encoded RNase H enzyme is
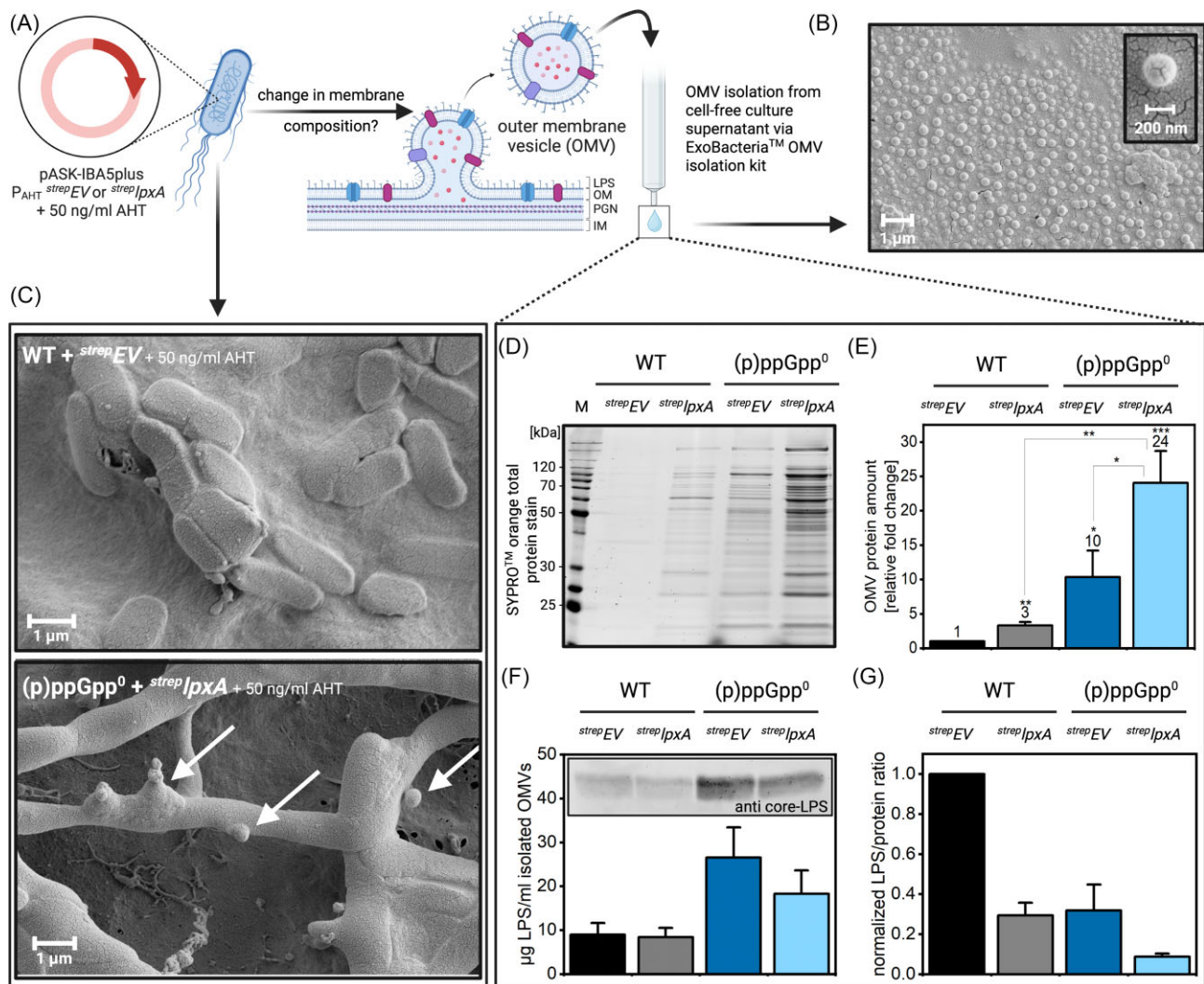
Figure 5. Overexpression of ^strep^lpxA increases OMV formation and affects its composition. **(A)** Changes in membrane composition can affect OMV formation. **(B)** Cryo-SEM analysis of isolated OMVs. **(C)** Cryo-SEM analysis of overnight overexpression cultures. Cells were washed three times with PCR-grade ddH$_2$O. Arrows indicate OMVs that are currently vesiculating from the cell. **(D)** SYPRO™ Orange stained SDS-PAGE of isolated OMVs. M: marker. **(E)** Quantification of OMV-associated proteins based on band intensities of SYPRO™ Orange stained SDS-PAGE. Error bars represent the SD; asterisks represent P-values of unpaired t-tests compared to WT carrying the EV or as indicated. **(F)** Immunological detection of OMV-associated core-LPS. Commercially available LPS was used for quantification. The bars represent the mean; the error bars the SD of three biological replicates. **(G)** The intensities of the LPS bands were divided by the intensities of the protein bands to calculate the LPS/protein ratio. Ratios were normalized to WT with EV. The bars represent the mean; the error bars the SD of three biological replicates.

seemingly unrelated to LPS biosynthesis, we considered ^strep^RnhB as a negative control in these experiments. Surprisingly, the protein strongly induced cell elongation comparable to that of LpxA (Fig. 6A). RnhB^strep^ (with the tag on the other end) had a significantly less pronounced effect than ^strep^RnhB in the WT. ^strep^RnhA that we then used as an additional control protein induced comparable cell elongation.

The (p)ppGpp^0 mutant was generally longer than the WT, and overproduction of ^strep^LpxA, ^strep^RnhB, and RnhB^strep^ substantially increased the length of the cell (Fig. 6A).

Changes in membrane permeability might accompany the overproduction of cell envelope biosynthesis enzymes. We tested this assumption using the fluorescent probe NPN that incorporates into compromised lipid bilayers resulting in strong fluorescence (Helander and Mattila-Sandholm 2000). As a positive control, cells were treated with 1 mM EDTA, which destabilizes the LPS layer by chelating divalent cations (Leive 1965). This destabilization led to a 1.5-fold increase in NPN uptake (P = .0004)

(Fig. 6B). The overproduction of ^strep^FabZ, ^strep^LpxD, ^strep^RnhB, RnhB^strep^, and ^strep^mCherry had no significant effect on NPN uptake. ^strep^MurA, ^strep^LpxA, and ^strep^LpxC increased the NPN uptake 1.75, 1.48, and 1.85 times, respectively (P = .0219, .0340, and .0004, respectively), whereas ^strep^RnhA decreased NPN uptake 0.57 times.

To ensure that cell length variations or other parameters did not affect the OD$_{600}$-based normalization, cells prepared for the NPN uptake assay were serially diluted, spotted on LB agar, and CFU/ml was determined (Fig. 6C). The overproduction of ^strep^FabZ, ^strep^LpxC, ^strep^LpxD, and ^strep^RnhA resulted in significantly lower CFU (P = .0013, .0018, .0014, and .0013, respectively), indicating that the results of the NPN uptake measurement might be underestimated for these strains. For ^strep^MurA and ^strep^LpxA, the number of CFU was comparable to that of the EV-containing cells, while the NPN uptake was significantly increased. In conclusion, the overproduction of LpxA and MurA, the first enzymes in LPS and PGN biosynthesis, respectively, seems to disturb membrane permeability.
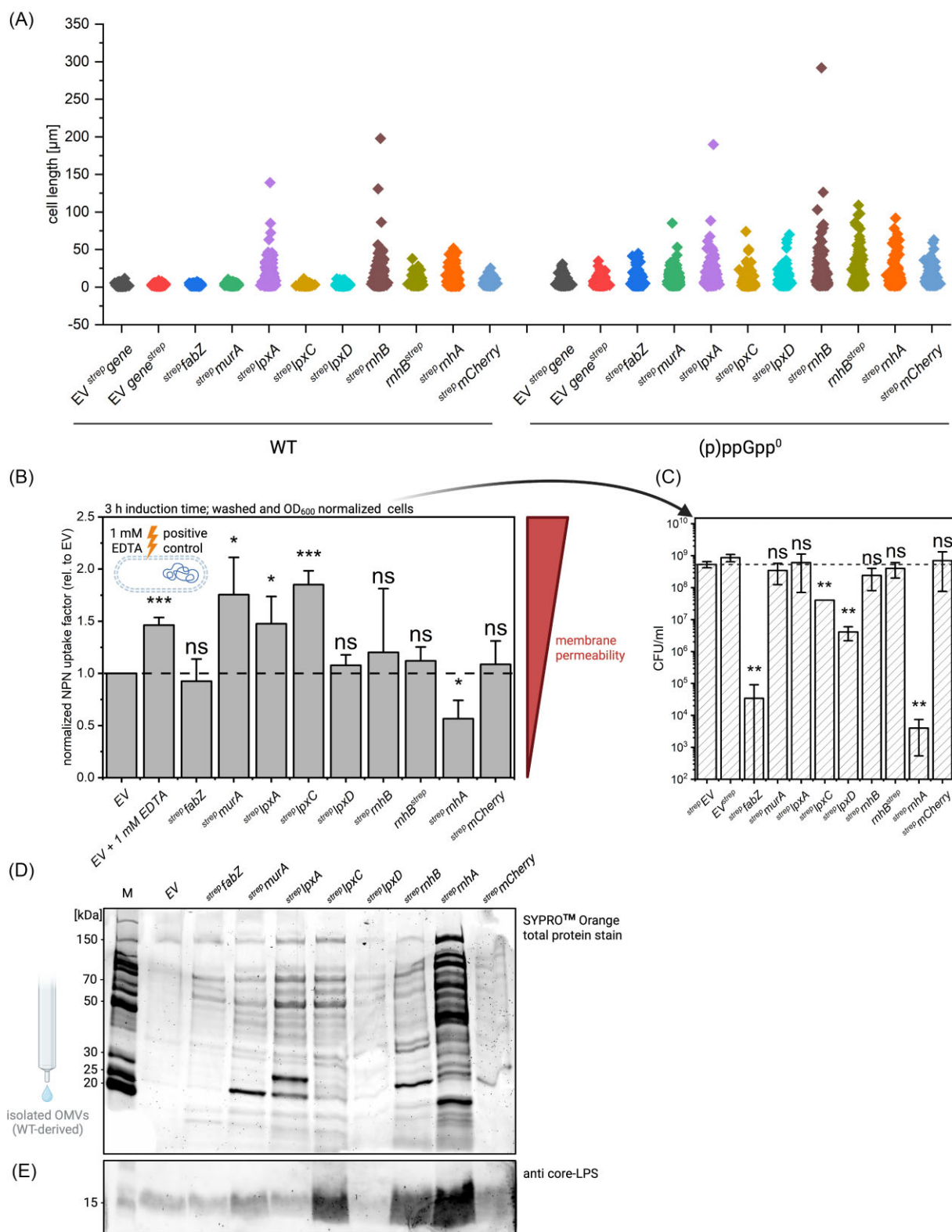
Figure 6. Assessment of cell length, membrane permeability, and OMV formation in response to protein overproduction. **(A)** WT or (p)ppGpp° cells overexpressing the indicated genes were cultured overnight and subjected to microscopic analysis to determine cell length. **(B)** WT cells harboring the indicated plasmids were cultured for 105 min, and overexpression was induced by addition of 50 ng/ml AHT for 3 h. The cells were washed and OD_{600}-normalized, and membrane permeability was assessed using the NPN uptake assay. A total of 1 mM EDTA, a known membrane disruptor, was used as a positive control to increase membrane permeability. NPN uptake factors were normalized to cells harboring the EV. Bars represent the mean; error bars represent the SD of three biological replicates; asterisks represent P-values of unpaired t-tests compared to WT with the EV. **(C)** OD_{600}-normalized cells used in (B) were serially diluted and spotted on LB agar to determine the CFU/ml. Bars represent the mean, error bars the SD of three biological replicates, and asterisks represent P-values of unpaired t-tests compared to WT with the EV. **(D)** Isolated OMVs from WT cells overexpressing the indicated genes for 18 h were subjected to SDS-PAGE and SYPRO™ Orange staining to visualize proteins. **(E)** These samples were also subjected to SDS-PAGE and Western transfer for immunological detection of core-LPS.

To assess whether proteins other than LpxA affect OMV formation, we tested several enzymes involved in cell envelope biosynthesis. ^strep^FabZ, ^strep^LpxD, and the control ^strep^mCherry did not affect vesiculation (Fig. 6D). Elevated amounts of OMVs were detected after ^strep^MurA, ^strep^LpxA, ^strep^LpxC, ^strep^RnhB, and ^strep^RnhA overproduction. OMVs derived from the WT overproducing ^strep^LpxC contained markedly more LPS (Fig. 6E) consistent with LpxC catalyzing the first committed step in LPS production. Strikingly, the OMVs after ^strep^RnhB or ^strep^RnhA overproduction also contained higher amounts of LPS, suggesting a role of RnhB and RnhA in membrane biogenesis. However, since the CFU count of the ^strep^RnhA overproduction strain was drastically reduced (Fig. 6C), the observed proteins might be a result of cell lysis, which is one of the common OMV biogenesis routes (Toyofuku et al. 2023).

RnhB is the secondary RNase H enzyme in *E. coli* and interacts with ppGpp

The presence of the *rnhB* gene in the same operon downstream of the *lpxA* gene (Fig. 7A) supported a connection to LPS biosynthesis because the organization of genes in an operon often indicates a functional relationship (Moreno-Hagelsieb 2015). This putative connection led us to investigate the activity of RnhB and its isoenzyme RnhA (Itaya 1990) in more detail. We employed a molecular beacon approach and confirmed that both enzymes could cleave an RNA:DNA hybrid (Figure S4, Supporting Information). Notably, RnhA exhibited ~1000 times higher RNase H activity than RnhB, suggesting that the first enzyme is the primary RNase H in *E. coli* and that the second one might have adopted alternative functions.

Along with the LPS biosynthesis enzymes (Fig. 2C), we examined RnhB and RnhA for ppGpp binding in crude cell extracts derived from the corresponding ASKA strains in the DRaCALA setup. RnhB was identified as a ppGpp binder (125 ± 11% ppGpp-binding rel. to RelA), whereas RnhA did not bind ppGpp (8 ± 6%) (Fig. 7B). The results were confirmed with purified strep-tagged proteins using thermal shift assays (Fig. 7C). For ^strep^RnhB, a clear shift in the melting curve in the presence ppGpp, but not in the presence of ATP, GTP, or GDP, indicated an RnhB–ppGpp interaction. In agreement with the DRaCALA assay, neither ppGpp nor the other nucleotides shifted the melting temperature of ^strep^RnhA.

Given the observed ppGpp binding, we asked whether the nucleotide affects the RNase H activity of RnhB. RnhB activity decreased with increasing concentrations of ATP, GTP, GDP, and ppGpp. At higher concentrations, the inhibitory effect of ppGpp was significantly more pronounced as compared to ATP, GTP, or GDP (Fig. 7D). At 2 mM nucleotide concentration, RnhB activity was 58%–68% in the presence of the other nucleotides, but only 25% in the presence of ppGpp. This finding supports an inhibitory effect of ppGpp on the RNase H activity of RnhB.

RNase H enzymes interact with LpxA and influence its activity

A previous high-throughput pull-down screen utilizing the ASKA strain collection reported a physical interaction between RnhB and LpxA (Arifuzzaman et al. 2006), which supports a role of RnhB in LPS biosynthesis. To collect evidence that RnhB affects LpxA activity *in vivo*, we cotransformed the ∆*rnhB* strain and the isogenic Keio WT strain (BW25113) with plasmid combinations coding for ^strep^*lpxA* and ^his^*rnhB* or the corresponding EVs. ^strep^mCherry served as control (Fig. 8A and B). During growth in a 96-well plate, we noticed that the ∆*rnhB* mutant reached higher cell densities

than the WT. However, there were no noticeable growth defects after the addition of inducers. We also applied the resazurin assay here, and the strain with both EVs was set as 100% viability. Overexpression of ^his^*rnhB* or ^strep^*lpxA* alone in the WT resulted in reduced cell viability. The coexpression of ^his^*rnhB* and ^strep^*lpxA* did not have an additive effect in Keio WT. In the ∆*rnhB* mutant, it was striking that neither ^his^*rnhB* nor ^strep^*lpxA* overexpression alone affected viability. On the contrary, the coexpression of both genes significantly reduced the viability of the ∆*rnhB* mutant to WT levels. These results suggest an *in vivo* effect of RnhB on LpxA with implications for the metabolism and redox potential of the cell.

We then asked whether the cellular steady-state LPS levels in the ∆*rnhB* and ∆*rnhA* mutants differed from the WT (Fig. 8C). We found that the LPS levels of the ∆*rnhB* and ∆*rnhA* strains were slightly lower in the exponential phase than in the WT (0.90 ± 0.08 and 0.79 ± 0.11, respectively). During transition to stationary phase, the LPS levels dropped in all strains (0.52 ± 0.05, 0.58 ± 0.18, and 0.6 ± 0.05 for WT, ∆*rnhB*, and ∆*rnhA*, respectively, with *P*-values of .0001, .0495, and .0440 when compared with each strain in exponential phase). In this phase, (p)ppGpp levels are highest in the cell (Varik et al. 2017). This result supports the model that (p)ppGpp inhibits LpxA and, thus LPS biosynthesis. In stationary phase, LPS levels remained low in the WT, whereas cellular LPS levels tended to be elevated in the mutants. Overall, the results suggest that RnhB and RnhA may influence LPS biosynthesis.

To corroborate a direct protein–protein interaction with LpxA *in vitro*, we used microscale thermophoresis (MST). The concentration of fluorescently labeled ^His^RnhB or ^His^RnhA was kept constant at 50 nM, while the concentrations of ^strep^LpxA or DNase I (negative control) were varied. Interaction results in a dose-dependent altered thermophoresis of the fluorescently labeled protein. The change compared to the unbound protein (∆FNorm) can be plotted against the concentration of the protein–ligand. Because ^strep^RnhB and ^strep^RnhA were thermally unstable (Fig. 7C), we searched for buffer conditions that stabilized the proteins in thermal shift experiments and used this buffer for MST measurements. It was apparent that the presence of ^strep^LpxA altered the thermophoresis behavior of ^His^RnhB and ^His^RnhA in a dose-dependent manner (Fig. 8D; representative MST traces in Figure S5, Supporting Information). The negative control DNase I did not affect the thermophoresis of ^His^RnhB or ^His^RnhA even at high concentrations. We also performed the reverse experiment with fluorescently labeled ^His^LpxA and ^strep^RnhB or ^strep^RnhA and obtained similar results, namely a LpxA–RnhB and LpxA–RnhA interaction and no interaction with DNase I (data not shown).

Furthermore, to show that interaction could also be detected in the PBS-T buffer recommended by the manufacturer, we fluorescently labeled ^His-SUMO^RnhB or ^His-SUMO^RnhA or the His-SUMO-tag (as a control). We incubated them with ^strep^LpxA or DNase I (Figure S6, Supporting Information). The fusion proteins remained stable under the assay conditions, presumably due to the SUMO fusion serving as a solubility tag. These experiments again supported a specific interaction between ^strep^LpxA and ^His-SUMO^RnhB or ^His-SUMO^RnhA. As expected, the His-SUMO-tag alone did not interact with LpxA or DNase I. In summary, three lines of independent MST experiments with different protein combinations in different buffers supported a direct physical interaction between LpxA and RnhA and LpxA and RnhB.

Given these interactions, we asked whether RnhB and RnhA affect the *in vitro* activity of LpxA. We used the same fluorescent LpxA activity assay that we had employed before and preincubated purified ^strep^RnhB, ^strep^RnhA, or DNase I at different concentrations with ^strep^LpxA at RT for 30 min and started the reaction by
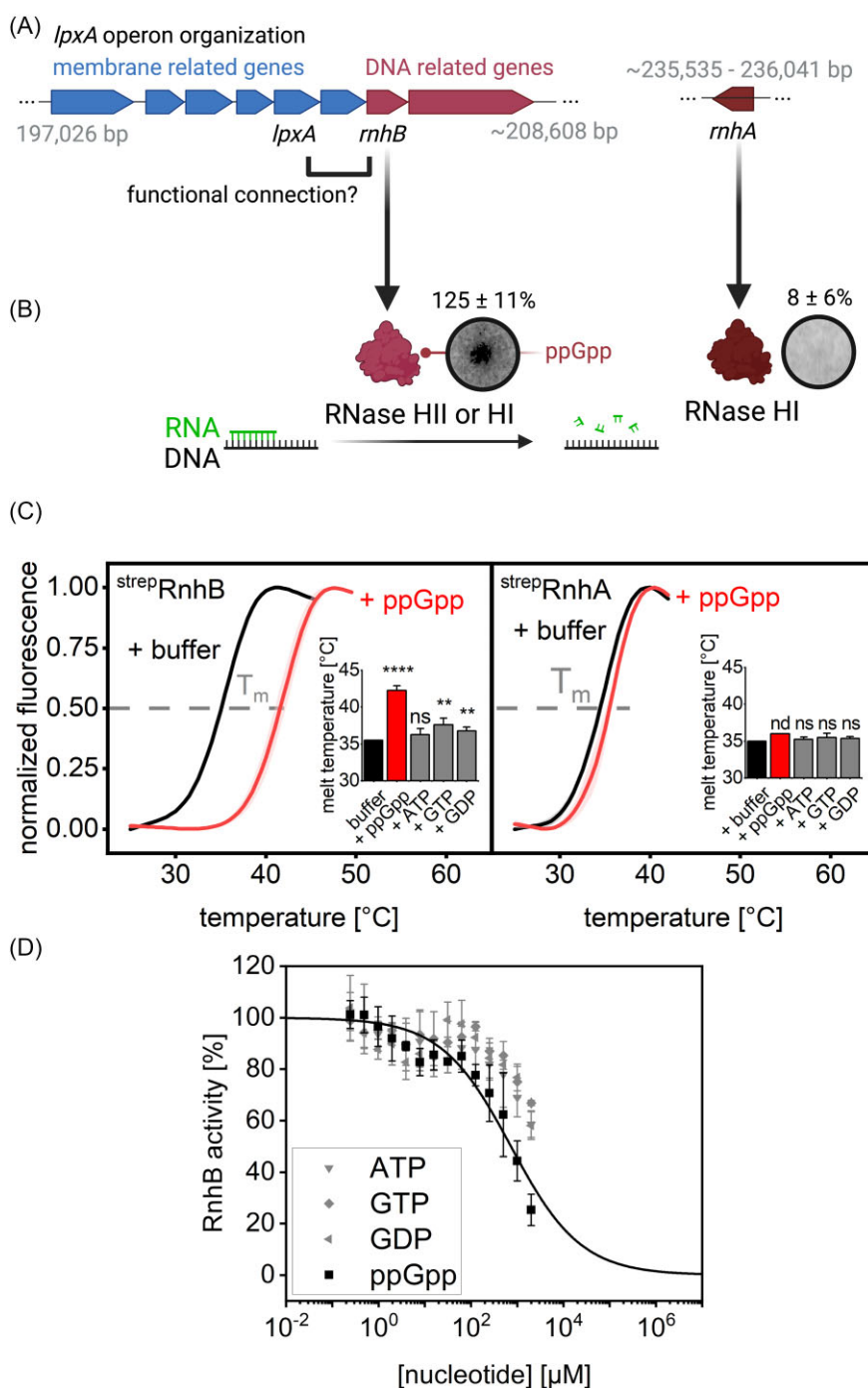
Figure 7. ppGpp binds and inhibits the RNase RnhB. **(A)** Representation of the *lpxA* operon. The *lpxA* and *rnhB* genes are encoded together in one operon. RnhA has the same catalytic activity as RnhB but is significantly more active. The *rnhA* gene is located at a different site in the genome. **(B)** The binding of ppGpp to ^{His}RnhB and ^{His}RnhA was determined by DRaCALA experiments. The values shown are the mean and SD of three biological replicates relative to ^{His}RelA binding capacity. **(C)** Melting curves of ^{strep}RnhB and ^{strep}RnhA in the presence of buffer and ppGpp, respectively. ATP, GTP, and GDP had a final concentration of 800 μM, and 2 μl of our ppGpp preparation was added (unknown concentration). The points represent the mean of the normalized melting curves of four technical replicates, and the error bands represent the SD. The line is a combined fit of the four melting curves to the Boltzmann equation. The bar graph shows the mean melting temperatures in the presence of buffer and different nucleotides (error bars are the SD). ^{strep}RnhB melting temperatures in the presence of buffer, ppGpp, ATP, GTP, or GDP were 35.5 ± 0°C, 42.3 ± 0.6°C, 36.3 ± 0.9°C, 37.6 ± 0.9°C, and 36.8 ± 0.5°C, respectively. Ns: nonsignificant shift compared to buffer as judged by *t*-test analysis or when the shift was ≤1°C. Nd: *P*-value could not be determined. Asterisks indicate the *P*-values of the unpaired *t*-tests. **(D)** RNase H activity of RnhB was determined in the presence of increasing nucleotide concentrations. Data points represent the mean, and error bars the SD of three technical replicates. The line represents a logistic fit with empirically determined limits. Reactions without nucleotide (control buffer was included) were used to normalize RnhB activity to 100% (upper limit of the fit). Reactions without RnhB were used to determine the lower limit of the fit. While all tested nucleotides had an inhibiting effect on the RNase H activity of RnhB, the effect of ppGpp was much stronger compared to the specificity controls ATP, GTP, and GDP.
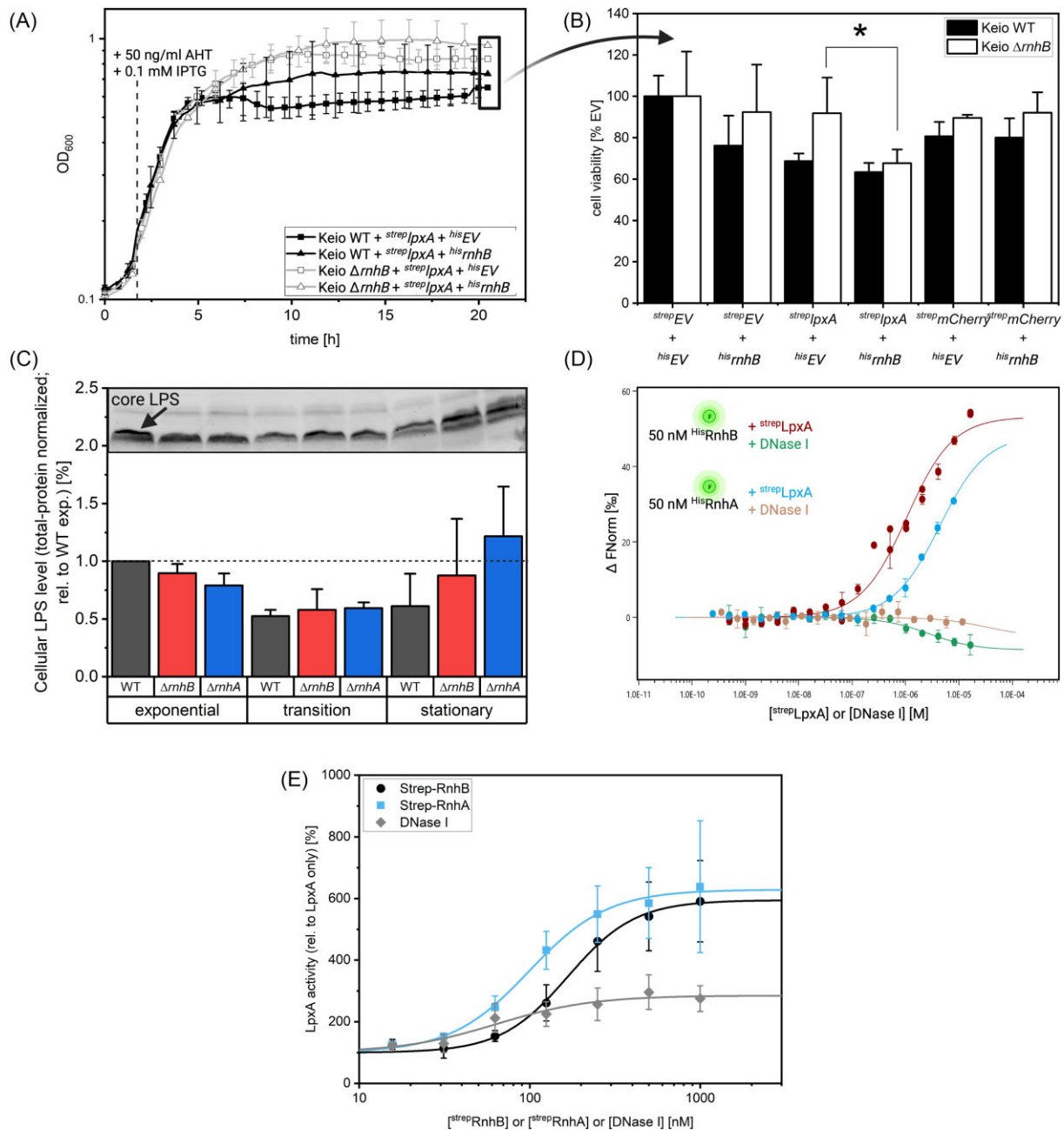
Figure 8. The RNases RnhB and RnhA interact with LpxA and increase its activity. **(A)** Growth curves in 96-well plates of Keio strains transformed with two plasmids. Cells were grown, and overexpression was induced after 105 min by adding AHT and IPTG. Data points represent the mean, and error bars represent the SD of four biological replicates. Not all data points are shown for clarity. ^{His}EV is pCA24N. **(B)** At the end of the growth curve, cell viability was determined by a resazurin assay, with viability normalized for each strain carrying both EVs. Bars and error bars represent the mean and SD of four biological replicates. The asterisk represents the *P*-value obtained by unpaired *t*-test. Viability after ^{his}rnhB or ^{strep}lpxA overexpression in the WT was 76 ± 15% with $P = .0353$ and 69% ± 4% with $P = .0011$, respectively. The viability of the WT with coexpression of ^{his}rnhB and ^{strep}lpxA was (63% ± 4%). The viability of the ΔrnhB strain with ^{his}rnhB or ^{strep}lpxA overexpression alone was 92% ± 23% with $P = .6444$ and 92 ± 17% with $P = .5743$, respectively. **(C)** Steady state cellular LPS levels of the Keio strains ΔrnhB, ΔrnhA, and their isogenic WT. Bacteria were harvested in the exponential phase (OD$_{600}$ of 0.5), in the transition phase when bacteria just ceased exponential growth, and in deep stationary phase (overnight cultures). Cells were boiled in SDS sample buffer and the samples were subjected to SDS-PAGE, Stain-Free™ activation of total protein, western transfer, and immunological detection of core LPS. Signal intensities for core LPS were determined and normalized to total-protein using the Stain-Free™ signal intensities detected on the same blot (internal loading control). WT in exponential phase was set to 1. Cellular LPS levels were lower in the transition and stationary phase compared to exponential phase. Compared to WT, cellular LPS levels of the ΔrnhB and ΔrnhA strains tended to be lower in exponential phase and higher in stationary phase. **(D)** MST data analysis. We evaluated changes in the fluorescence signal of the labeled protein to its unbound state. While maintaining fixed concentrations of ^{His}RnhB and ^{His}RnhA, we systematically varied the concentrations of ^{strep}LpxA and DNAse I to determine their effect on the thermophoresis of the labeled protein. The MST traces are shown in Figure S5 (Supporting Information). ^{strep}LpxA had a measurable effect on ^{His}RnhB thermophoresis at ~128 nM, and ΔFNorm reached a value of ~55. ^{His}RnhA thermophoresis was affected, starting at ~500 nM of ^{strep}LpxA, and ΔFNorm reached ~30. **(E)** Effect of different proteins on the activity of LpxA. We incubated LpxA with ^{strep}RnhB, ^{strep}RnhA, or DNase I for 30 min at RT before initiating the LpxA assay by adding the enzymes. The relative activity of LpxA was calculated from the initial velocities (LpxA alone is 100%). The final concentration of LpxA was 10 nM (calculated as trimer), and the indicated protein–ligand concentrations were the final concentrations in the assay. The graph's data points and error bars represent the mean and SD of three technical replicates. The line represents the logistic fit.

adding the preincubated proteins. The reaction with LpxA alone was set to 100% activity. As expected, LpxA activity was not detected with [strep]RnhB and [strep]RnhA alone (data not shown). The presence of DNase I in the assay stimulated LpxA activity about 2-fold. A much more substantial, about 6-fold dose-dependent increase of LpxA activity was found in the presence of [strep]RnhB or [strep]RnhA (Fig. 8E). Altogether, these results suggest that the interaction with RnhB or RnhA influences LpxA activity and generates diverse membrane-associated phenotypes in *E. coli*.

Discussion

Intricate control of PL, PGN, and LPS biosynthesis involves (p)ppGpp

A role of (p)ppGpp in regulating cell envelope biogenesis in *E. coli* has long been recognized. For example, (p)ppGpp inhibits FabZ, which catalyzes the first step of PL biosynthesis, as well as a late step of PGN biosynthesis (Stein and Bloch 1976, Ramey and Ishiguro 1978). LPS molecules are the third pillar of the Gram-negative cell envelope. The biosynthetic pathways of PL, PGN, and LPS share the same substrates and are tightly intertwined and highly regulated (Fig. 1B). One indication of this functional linkage is that LpxB (LPS biosynthesis) copurifies with PL (Metzger and Raetz 2009). It is also known that the cellular activities of FabZ (PL biosynthesis) and LpxC (LPS biosynthesis) are coregulated *in vivo*. Both enzymes occur in a LapB-anchored membrane protein complex, which might control the substrate flux into the divergent biosynthetic pathways (Möller et al. 2023). When FabZ activity is impaired, LpxC is less abundant in the cell, and when *fabZ* is overexpressed, LpxC levels are also upregulated (Zeng et al. 2013, Thomanek et al. 2019). The protease FtsH is responsible for the controlled turnover of LpxC (and LpxD) to balance LPS production according to the cellular demand (Ogura et al. 1999, Möller et al. 2023). Inhibition of lipid A biosynthesis results in the accumulation of LpxC (Sorensen et al. 1996), and FtsH-mediated degradation of LpxC is growth-phase dependent (Schäkermann et al. 2013). During fast growth (high LPS demand), LpxC is stable, whereas, during slow growth (low LPS demand), LpxC is rapidly degraded. Notably, this pattern is reversed in a (p)ppGpp^0 mutant, indicating a vital role of the growth-phase-dependent signaling nucleotide in this process.

Meanwhile, a dynamic membrane protein complex comprised of LapB (YciM) and YejM (LapC, PgbA) has been implicated in the sensing of LPS precursors and coordination of LpxC turnover (Biernacka et al. 2020, Fivenson and Bernhardt 2020, Guest et al. 2020, Shu and Mi 2022). It has also been shown that the lethality of a Δ*lapB* mutant (too much LPS production) can be rescued by overexpressing *murA* (PGN biosynthesis), which limits the availability of UDP-GlcNAc for the LPS pathway (Klein et al. 2014). All these reports demonstrate a tight cross-regulation of PL, PGN, and LPS biosynthesis and involvement of (p)ppGpp at various levels, presumably to allocate and save resources and to prevent biosynthesis of dispensable building blocks under stringent conditions.

(p)ppGpp influences LpxA activity

To uncover a direct role of (p)ppGpp in LPS biosynthesis, we conducted DRaCALA experiments with crude extracts from the ASKA overexpression strains. The results suggested that LpxA or an associated protein binds ppGpp in cell lysate (Fig. 2C). This interaction or a hit with any other LPS-producing protein was not reported in a previous proteome-wide DRaCALA screen (Zhang et al. 2018). This absence can at least partly be explained by dif-

ferent culture conditions, as the authors induced overexpression in overnight cultures, whereas we used exponential cells. In our case, the cellular (p)ppGpp concentration would be lower due to the earlier growth phase. Lower concentrations should facilitate the detection of weak interactions because the lower abundance of (p)ppGpp in the crude extracts would not be able to compete for binding partners with the added radioactive ppGpp. A low (p)ppGpp binding affinity of a protein from an essential pathway would meet the expectation because such enzymes should be inhibited only at high nucleotide concentrations (Steinchen et al. 2020).

In a purified system using the thermal shift assay, which is well suited for detecting protein–nucleotide interactions (Kopra et al. 2022), we were unable to confirm the LpxA–ppGpp interaction (Fig. 2D). Most likely, some factor available in the cell lysate but not in the biochemical assay mediated the apparent interaction in the DRaCALA assay. The most likely candidates are acyl-ACP, the fatty acid chain donor for LPS biosynthesis, and the newly identified LpxA interactor RnhB because both proteins were able to bind (p)ppGpp *in vivo* and *in vitro* (Figs 2E and 7C). ACP also appeared to bind other nucleotides. ACP is one of the most abundant proteins in *E. coli*, with 60 000 to more than 350 000 molecules/cell (vanden Boom and Cronan 1989, Li et al. 2014). The enormous abundance in cell lysates might explain why the DRaCALA assay failed to detect strong binding.

A continuous fluorescent LpxA assay (Jenkins and Dotson 2012) with purified components showed that (p)ppGpp inhibits LpxA activity *in vitro* in a dose–response manner (Fig. 3E and F). Since (p)ppGpp did not interact directly with LpxA, we assume that it exerts its inhibitory action via its substrate ACP. The extent of inhibition appeared to be highly dependent on the concentration of acyl-ACP, the most challenging component to prepare for this assay. At low acyl-ACP concentrations, the inhibitory effect of (p)ppGpp was lower than at high concentrations. In the cellular context, (p)ppGpp might serve as an emergency brake that inhibits the LpxA-catalyzed reaction under changing environmental conditions.

Overproduction of LpxA, RnhB, and RnhA induces cell elongation

Previous studies have shown that cells lacking (p)ppGpp are longer and produce more biomass than WT cells (Traxler et al. 2008, Büke et al. 2022, Lee et al. 2023). This correlation was associated with increased gene expression in several metabolic pathways. Conversely, increased levels of (p)ppGpp negatively affect the synthesis of cellular macromolecules such as DNA, cell walls, and membranes (Traxler et al. 2008). Our interest in the connection between (p)ppGpp and LPS biosynthesis prompted us to ask what happens when LpxA, the first essential enzyme in this pathway, is overproduced. Previously, inhibition of *lxpA* expression using clustered regularly interspaced short palindromic repeats interference (CRISPRi) was shown to induce the stringent response and cell elongation (Roghanian et al. 2019). The effects were exacerbated in the (p)ppGpp^0 mutant up to the point of cell lysis. We observed filamentous cells in response to LpxA overproduction in *E. coli* W3110, and this effect was more pronounced in a (p)ppGpp^0 mutant (Fig. 4C). Neither FabZ, MurA, LpxC, nor LpxD overproduction affected cell length as severely as LpxA (Fig. 6A). Thus, the overproduction of LPS itself (by overexpression of *lpxC*) did not seem to be responsible for cell elongation. Since the LpxA forward reaction is thermodynamically unfavorable, we assumed that substrates might be redirected to the PL or PGN pathway,

causing an imbalance of membrane components (Anderson et al. 1993). Although it certainly cannot fully explain the extent of cell elongation in the *lpxA* overexpression strain, the slight elongation upon *murA* overexpression (Table S4, Supporting Information) suggests that some precursors might be redirected toward PGN biosynthesis. In agreement with conclusions from the CRISPRi screen (Roghanian et al. 2019), the dense interconnection between cell envelope biosynthesis processes makes it difficult to attribute a single gene to the filamentous phenotype.

A fortuitous finding of our study was that the overproduction of the RNAses RnhB and RnhA caused filamentous growth in WT and (p)ppGpp[0] strains like *lpxA* overexpression. This finding is in concert with a previous study reporting a protein–protein interaction between LpxA and RnhB (Arifuzzaman et al. 2006) and suggested a functional relationship between these proteins and a possible moonlighting function of RnhB in LPS biosynthesis.

Interfering with early steps of LPS biosynthesis induces OMV formation

It is known that *E. coli* mutants with truncated LPS molecules tend to increase OMV formation (Kulp et al. 2015). The accumulation of PGN fragments and LPS molecules also leads to hypervesiculation (Schwechheimer et al. 2014). We isolated OMVs from stationary cultures when (p)ppGpp levels are naturally high and when OMV yields are known to be highest (Klimentová and Stulík 2015). We found that LpxA overproduction increased OMV formation, which was much more pronounced in the (p)ppGpp[0] mutant. Interestingly, the LPS/protein ratio of OMVs from this strain was greatly reduced compared to the WT and decreased in both strains in response to LpxA overproduction (Fig. 5F and G). Thus, the cells did not appear to secrete excess LPS by OMVs. This was different upon overproduction of LpxC, which drives the forward reaction in LPS biosynthesis. Here, the relative LPS amount was much higher (Fig. 6E).

In contrast, overproduced LpxD catalyzing the next step did not affect OMV formation and LPS level (Fig. 6D and E), suggesting that the initial two LPS biosynthesis enzymes serve as checkpoints in membrane homeostasis. The unexpected finding that *rnhB* overexpression increases OMV formation and LPS levels provided another line of evidence that the secondary RNase H enzyme plays a role in LPS biosynthesis in concert with LpxA. Massive OMV production in the *rnhA* expression strain is probably due to unrelated reasons, e.g. toxicity and cell lysis due to elevated levels of the highly active primary RNase H.

Moonlighting functions of the RNase H enzymes RnhB and RnhA

First indications that RnhB might play a role in LPS biogenesis derived from the genetic context of the *rnhB* gene in the *E. coli lpxA* operon (Fig. 7A) and from global pull-down experiments showing an interaction between LpxA and RnhB (Arifuzzaman et al. 2006). This interaction was confirmed in the present study by MST, a very sensitive biochemical assay (Jerabek-Willemsen et al. 2011). Of note, this interaction was not seen in a recent bacterial two-hybrid screen where RnhB was considered a negative control because it was seemingly unrelated to LPS and PL biosynthesis functions (Möller et al. 2023). The missed interaction is most likely due to attached adenylate cyclase domains shielding the binding sites.

Proteins with additional functions not directly related to their enzymatic tasks are collectively called moonlighting proteins (Jeffery 1999). An example from *B. subtilis* involving several RNases is a protein complex composed of the two glycolytic enzymes phos-

phofructokinase and enolase and the RNA-processing enzymes RNAse J1, Rny, and polynucleotide phosphorylase (Commichau et al. 2009). In the context of our study, it is most interesting that RnhB was recently reported to activate Ugd, an enzyme required for LPS modification (Rodionova et al. 2020). Since RnhB is the secondary RNase H in *E. coli*, it is probably free to evolve new functionalities.

Different bacteria seem to have developed different strategies to modulate LpxA activity. In *Francisella tularensis*, RipA stabilizes LpxA levels and supports adaptation to the host cell environment (Miller et al. 2014). A modulator of LpxA in *Cronobacter sakazakii* was named LabP. A Δ*labP* mutant exhibited several membrane-related phenotypes, including increased PL production, surface hydrophobicity, membrane permeability (determined by NPN uptake factor), and strong cell aggregation (Kim et al. 2018). In our study, several RnhB-related phenotypes in *E. coli* were also associated with an altered cell envelope *in vivo*, and RnhB was found to modulate LpxA activity *in vitro*.

Many bacterial genomes encode several RNase H enzymes, and the physiological significance of the multiplicity of RNases H has remained a mystery. Surprisingly, *E. coli* and *B. subtilis* mutants lacking all RNase H genes are viable, albeit showing a temperature-sensitive growth phenotype. It was concluded that RNase H activity is dispensable for growth but involved in critical cellular processes (Tadokoro and Kanaya 2009). There is emerging evidence that proteins from metabolic pathways, such as carbohydrate or nitrogen metabolism, have moonlighting functions to coordinate cell division and DNA replication with metabolism (Sperber and Herman 2017). Our results add another piece of evidence in this context, as they suggest a link between replication or nucleotide repair by RnhB and membrane biosynthesis by LpxA.

The interpretation of the phenotypes observed in this study is complicated by the essentiality and interconnection of the cell envelope biosynthesis pathways. It is known that manipulation of pathways with common substrates can elicit pleiotropic effects in other directions (Sperber and Herman 2017). Interesting examples are *E. coli* OpgG and OpgH, which are responsible for synthesizing osmoregulated periplasmic glucans in a process requiring acyl-ACP (Therisod et al. 1986, Bontemps-Gallo et al. 2017). OpgH also has a moonlighting function as a regulator of cell size, acting as an inhibitor of FtsZ ring formation in the presence of UDP-glucose (nutrient-rich conditions) (Hill et al. 2013). The Ugd enzyme, which RnhB activates, also uses UDP-glucose for its reaction, suggesting that the regulatory system may be even more complex (Rodionova et al. 2020). Since acyl-ACP is also used in the biosynthesis of PL and LPS, it is conceivable that the availability of acyl-ACP and UDP-glucose orchestrates various metabolic pathways by the interaction of metabolic enzymes with signaling nucleotides and moonlighting enzymes.

Authors' contributions

Simon Brückner (Data curation, Formal analysis, Investigation, Methodology, Visualization, Writing—original draft), Fabian Müller (Data curation, Formal analysis, Investigation, Methodology, Visualization), Laura Schadowski (Data curation, Investigation), Tyll Kalle (Data curation, Investigation), Sophia Weber (Data curation, Investigation), Emily C. Marino (Data curation, Investigation, Writing—review & editing), Blanka Kutscher (Data curation, Investigation), Anna-Maria Möller (Conceptualization, Writing—review & editing), Sabine Adler (Data curation, Investigation, Methodology), Dominik Begerow (Resources), Wieland Steinchen (Resources), Gert Bange (Conceptualization, Resources),

Supplementary data

Supplementary data is available at *FEMSML* online.

Conflict of interest statement. None declared

References

Anderson BW, Fung DK, Wang JD. Regulatory themes and variations by the stress-signaling nucleotide alarmones (p)ppGpp in bacteria. *Annu Rev Genet* 2021;**55**:115–33.

Anderson MS, Bull HG, Galloway SM *et al.* UDP-N-acetylglucosamine acyltransferase of *Escherichia coli*. The first step of endotoxin biosynthesis is thermodynamically unfavorable. *J Biol Chem* 1993;**268**:19858–65.

Arifuzzaman M, Maeda M, Itoh A *et al.* Large-scale identification of protein–protein interaction of *Escherichia coli* K-12. *Genome Res* 2006;**16**:686–91.

Biernacka D, Gorzelak P, Klein G *et al.* Regulation of the first committed step in lipopolysaccharide biosynthesis catalyzed by LpxC requires the essential protein LapC (YejM) and HslVU protease. *IJMS* 2020;**21**:9088.

Bontemps-Gallo S, Bohin J-P, Lacroix J-M. Osmoregulated periplasmic glucans. *EcoSal Plus* 2017;**7**. https://doi.org/10.1128/ecosalplus.ESP-0001-2017.

Büke F, Grilli J, Cosentino Lagomarsino M *et al.* ppGpp is a bacterial cell size regulator. *Curr Biol* 2022;**32**:870–7.

Chung CT, Niemela SL, Miller RH. One-step preparation of competent *Escherichia coli*: transformation and storage of bacterial cells in the same solution. *Proc Natl Acad Sci USA* 1989;**86**:2172–5.

Commichau FM, Rothe FM, Herzberg C *et al.* Novel activities of glycolytic enzymes in *Bacillus subtilis*: interactions with essential proteins involved in mRNA processing. *Mol Cell Proteomics* 2009;**8**:1350–60.

Corona A, Tramontano E. RNase H polymerase-independent cleavage assay for evaluation of RNase H activity of reverse transcriptase enzymes. *Bio-Protocol* 2015;**5**:e1561.

Corrigan RM, Bellows LE, Wood A *et al.* ppGpp negatively impacts ribosome assembly affecting growth and antimicrobial tolerance in Gram-positive bacteria. *Proc Natl Acad Sci USA* 2016;**113**: E1710–9.

Fivenson EM, Bernhardt TG. An essential membrane protein modulates the proteolysis of LpxC to control lipopolysaccharide synthesis in *Escherichia coli*. *Mbio* 2020;**11**:e00939–20.

Flugel RS, Hwangbo Y, Lambalot RH *et al.* Holo-(acyl carrier protein) synthase and phosphopantetheinyl transfer in *Escherichia coli*. *J Biol Chem* 2000;**275**:959–68.

Guest RL, Samé Guerra D, Wissler M *et al.* YejM modulates activity of the YciM/FtsH protease complex to prevent lethal accumulation of lipopolysaccharide. Gottesman S (ed.). *Mbio* 2020;**11**:e00598–20.

Guo Y, Ji F, Qiao J *et al.* Overexpression of the key genes in the biosynthetic pathways of lipid A and peptidoglycan in *Escherichia coli*. *Biotech and App Biochem* 2023;**70**:374–86.

Helander IM, Mattila-Sandholm T. Fluorometric assessment of Gram-negative bacterial permeabilization. *J Appl Microbiol* 2000;**88**:213–9.

Hill NS, Buske PJ, Shi Y *et al.* A moonlighting enzyme links *Escherichia coli* cell size with central metabolism. *PLoS Genet* 2013;**9**:e1003663.

Irving SE, Choudhury NR, Corrigan RM. The stringent response and physiological roles of (pp)pGpp in bacteria. *Nat Rev Microbiol* 2021;**19**:256–71.

Itaya M. Isolation and characterization of a second RNase H (RNase HII) of *Escherichia coli* K-12 encoded by the *rnhB* gene. *Proc Natl Acad Sci USA* 1990;**87**:8587–91.

Jeffery CJ. Moonlighting proteins. *Trends Biochem Sci* 1999;**24**:8–11.

Jenkins RJ, Dotson GD. A continuous fluorescent enzyme assay for early steps of lipid A biosynthesis. *Anal Biochem* 2012;**425**:21–7.

Jerabek-Willemsen M, Wienken CJ, Braun D *et al.* Molecular interaction studies using microscale thermophoresis. *Assay Drug Dev Technol* 2011;**9**:342–53.

Jiang Y, Chan CH, Cronan JE. The soluble acyl-acyl carrier protein synthetase of *Vibrio harveyi* B392 is a member of the medium chain acyl-CoA synthetase family. *Biochemistry* 2006;**45**:10008–19.

Kanjee U, Ogata K, Houry WA. Direct binding targets of the stringent response alarmone (p)ppGpp. *Mol Microbiol* 2012;**85**:1029–43.

Kim S, Yoon H, Ryu S. New virulence factor CSK29544_02616 as LpxA binding partner in *Cronobacter sakazakii*. *Sci Rep* 2018;**8**:835.

Kim Y, Prestegard JH. Refinement of the NMR structures for acyl carrier protein with scalar coupling data. *Proteins* 1990;**8**:377–85.

Klein G, Kobylak N, Lindner B *et al.* Assembly of lipopolysaccharide in *Escherichia coli* requires the essential LapB heat shock protein. *J Biol Chem* 2014;**289**:14829–53.

Klimentová J, Stulík J. Methods of isolation and purification of outer membrane vesicles from Gram-negative bacteria. *Microbiol Res* 2015;**170**:1–9.

Kopra K, Valtonen S, Mahran R *et al.* Thermal shift assay for small GTPase stability screening: evaluation and suitability. *IJMS* 2022;**23**:7095.

Kulp A, Kuehn MJ. Biological functions and biogenesis of secreted bacterial outer membrane vesicles. *Annu Rev Microbiol* 2010;**64**:163–84.

Kulp AJ, Sun B, Ai T *et al.* Genome-wide assessment of outer membrane vesicle production in *Escherichia coli*. *PLoS ONE* 2015;**10**:e0139200.

Lee JB, Kim SK, Han D *et al.* Mutating both *relA* and *spoT* of enteropathogenic *Escherichia coli* E2348/69 attenuates its virulence and induces interleukin 6 *in vivo*. *Front Microbiol* 2023;**14**:1121715.

Leive L. Release of lipopolysaccharide by EDTA treatment of *E. coli*. *Biochem Biophys Res Commun* 1965;**21**:290–6.

Li G-W, Burkhardt D, Gross C *et al*. Quantifying absolute protein synthesis rates reveals principles underlying allocation of cellular resources. *Cell* 2014;**157**:624–35.

Lundstedt E, Kahne D, Ruiz N. Assembly and maintenance of lipids at the bacterial outer membrane. *Chem Rev* 2021;**121**:5098–123.

McMillan HM, Kuehn MJ. The extracellular vesicle generation paradox: a bacterial point of view. *EMBO J* 2021;**40**:e108174.

Metzger LE, Raetz CRH. Purification and characterization of the lipid A disaccharide synthase (LpxB) from *Escherichia coli*, a peripheral membrane protein. *Biochemistry* 2009;**48**:11559–71.

Miller CN, Steele SP, Brunton JC *et al*. Extragenic suppressor mutations in Δ*ripA* disrupt stability and function of LpxA. *BMC Microbiol* 2014;**14**:336.

Möller A-M, Brückner S, Tilg L-J *et al*. LapB (YciM) orchestrates protein–protein interactions at the interface of lipopolysaccharide and phospholipid biosynthesis. *Mol Microbiol* 2023;**119**:29–43.

Moreno-Hagelsieb G. The power of operon rearrangements for predicting functional associations. *Comput Struct Biotechnol J* 2015;**13**:402–6.

Ogura T, Inoue K, Tatsuta T *et al*. Balanced biosynthesis of major membrane components through regulated degradation of the committed enzyme of lipid A biosynthesis by the AAA protease FtsH (HflB) in *Escherichia coli*. *Mol Microbiol* 1999;**31**:833–44.

Prestegard JH, Kim Y. Refinement of the NMR structures for acyl carrier protein with scalar coupling data. *Proteins* 1993;**8**:377–85.

Pulschen AA, Fernandes AZN, Cunha AF *et al*. Many birds with one stone: targeting the (p)ppGpp signaling pathway of bacteria to improve antimicrobial therapy. *Biophys Rev* 2021;**13**:1039–51.

Raetz CRH, Roderick SL. A left-handed parallel *β* helix in the structure of UDP-N-acetylglucosamine acyltransferase. *Science* 1995;**270**:997–1000.

Ramey WD, Ishiguro EE. Site of inhibition of peptidoglycan biosynthesis during the stringent response in *Escherichia coli*. *J Bacteriol* 1978;**135**:71–7.

Rizzo J, Gifford LK, Zhang X *et al*. Chimeric RNA–DNA molecular beacon assay for ribonuclease H activity. *Mol Cell Probes* 2002;**16**:277–83.

Roderick SL. UDP N-acetylglucosamine acyltransferase. Protein Data Bank, 1995. https://doi.org/10.2210/pdb1LXA/pdb.

Rodionova IA, Zhang Z, Aboulwafa M *et al*. UDP-glucose dehydrogenase Ugd in *E. coli* is activated by Gmd and RffD, is inhibited by CheY, and regulates swarming. *bioRxiv* 2020. https://doi.org/10.1101/2020.01.08.899336.

Roghanian M, Semsey S, Løbner-Olesen A *et al*. (p)ppGpp-mediated stress response induced by defects in outer membrane biogenesis and ATP production promotes survival in *Escherichia coli*. *Sci Rep* 2019;**9**:2934.

Roujeinikova A, Simon WJ, Gilroy J *et al*. Structural studies of fatty acyl-(acyl carrier protein) thioesters reveal a hydrophobic binding cavity that can expand to fit longer substrates. *J Mol Biol* 2007;**365**:135–45.

Roujeinikova A. . Protein Data Bank, 2006. https://doi.org/10.2210/pdb2FAC/pdb.

Sambrook J, Russell DW. *Molecular Cloning: A Laboratory Manual*. Cold Spring Harbor: Cold Spring Harbor Laboratory Press, 2001.

Schäkermann M, Langklotz S, Narberhaus F. FtsH-mediated coordination of lipopolysaccharide biosynthesis in *Escherichia coli* correlates with the growth rate and the alarmone (p)ppGpp. *J Bacteriol* 2013;**195**:1912 LP–1919.

Schwechheimer C, Kuehn MJ. Outer-membrane vesicles from Gram-negative bacteria: biogenesis and functions. *Nat Rev Microbiol* 2015;**13**:605–19.

Schwechheimer C, Kulp A, Kuehn MJ. Modulation of bacterial outer membrane vesicle production by envelope structure and content. *BMC Microbiol* 2014;**14**:324.

Shu S, Mi W. Regulatory mechanisms of lipopolysaccharide synthesis in *Escherichia coli*. *Nat Commun* 2022;**13**:4576.

Silhavy TJ, Kahne D, Walker S. The bacterial cell envelope. *Cold Spring Harb Perspect Biol* 2010;**2**:a000414.

Sorensen PG, Lutkenhaus J, Young K *et al*. Regulation of UDP-3-O-[R-3-hydroxymyristoyl]-N-acetylglucosamine deacetylase in *Escherichia coli*: the second enzymatic step of lipid A biosynthesis. *J Biol Chem* 1996;**271**:25898–905.

Sperber AM, Herman JK. Metabolism shapes the cell. *J Bacteriol* 2017;**199**:e00039–17.

Stein JP, Bloch KE. Inhibition of *E. coli* *β*-hydroxydecanoyl thioester dehydrase by ppGpp. *Biochem Biophys Res Commun* 1976;**73**:881–4.

Steinchen W, Schuhmacher JS, Altegoer F *et al*. Catalytic mechanism and allosteric regulation of an oligomeric (p)ppGpp synthetase by an alarmone. *Proc Natl Acad Sci USA* 2015;**112**:13348 LP–13353.

Steinchen W, Zegarra V, Bange G. (p)ppGpp: magic modulators of bacterial physiology and metabolism. *Front Microbiol* 2020;**11**:2072.

Tadokoro T, Kanaya S. Ribonuclease H: molecular diversities, substrate binding domains, and catalytic mechanism of the prokaryotic enzymes. *FEBS J* 2009;**276**:1482–93.

Therisod H, Weissborn AC, Kennedy EP. An essential function for acyl carrier protein in the biosynthesis of membrane-derived oligosaccharides of *Escherichia coli*. *Proc Natl Acad Sci USA* 1986;**83**:7236–40.

Thomanek N, Arends J, Lindemann C *et al*. Intricate crosstalk between lipopolysaccharide, phospholipid and fatty acid metabolism in *Escherichia coli* modulates proteolysis of LpxC. *Front Microbiol* 2019;**9**:3285.

Toyofuku M, Schild S, Kaparakis-Liaskos M *et al*. Composition and functions of bacterial membrane vesicles. *Nat Rev Microbiol* 2023;**21**:415–430.

Traxler MF, Summers SM, Nguyen HT *et al*. The global, ppGpp-mediated stringent response to amino acid starvation in *Escherichia coli*. *Mol Microbiol* 2008;**68**:1128–48.

vanden Boom T, Cronan JE. Genetics and regulation of bacterial lipid metabolism. *Annu Rev Microbiol* 1989;**43**:317–43.

Varik V, Oliveira SRA, Hauryliuk V *et al*. HPLC-based quantification of bacterial housekeeping nucleotides and alarmone messengers ppGpp and pppGpp. *Sci Rep* 2017;**7**:11022.

Wang B, Dai P, Ding D *et al*. Affinity-based capture and identification of protein effectors of the growth regulator ppGpp. *Nat Chem Biol* 2019;**15**:141–50.

Zeng D, Zhao J, Chung HS *et al*. Mutants resistant to LpxC inhibitors by rebalancing cellular homeostasis. *J Biol Chem* 2013;**288**:5475–86.

Zhang Y, Zborníková E, Rejman D *et al*. Novel (p)ppGpp binding and metabolizing proteins of *Escherichia coli*. Swanson MS (ed.). *Mbio* 2018;**9**:e02188–17.